

UNIVERSITY OF WEST BOHEMIA
FACULTY OF APPLIED SCIENCES
DEPARTMENT OF MECHANICS

BACHELOR THESIS

EXPERIMENTAL ANALYSIS OF SACRAL BONE FIXATORS

PLZEŇ, 2015

JANA HARTLOVÁ

I hereby declare that this thesis is my own work, and it does not contain other people's work without this being stated; and that the bibliography contains all the literature that I have used in writing the thesis, and that all references refer to this bibliography.

Plzeň, 30. 5. 2015

Jana Hartlová

ACKNOWLEDGMENT

First and foremost I would like to express my gratitude to my supervisor Ing. Libor Lobovský, Ph.D. for his guidance, patience and encouragement over the last two years. His attitude to the work motivated me a lot.

I would like to thank MUDr. Martin Salášek, Ph.D. who provided me with important knowledge in the field of pelvic anatomy and orthopaedics and who assisted in the preparation of the experiments. I would also like to thank Ing. Jan Krystek, Ph.D. for assistance in the experimental measurements and Ing. Jan Heczko for helpful discussions and advice.

ABSTRACT

The aim of the thesis is a comparison of four fixators used for stabilisation of unilateral transforaminal sacral fracture. Their stability is examined during experimental measurements performed on orthopaedic models of pelvis. For the evaluation of the experimental data the methods of photogrammetry and digital image correlation were used. The photogrammetric software was tested and its accuracy was determined. In order to analyse the stability of the fixators, the dislocations of selected points at the dorsal surface of the sacrum were quantified.

Keywords Sacrum, iliosacral screw, transiliac internal fixator, transiliac plate, sacral bar, experimental analysis, photogrammetry, image correlation.

ABSTRAKT

Práce se zaměřuje zejména na srovnání čtyř typů fixátorů používaných pro jednostrannou transforaminální zlomeninu křížové kosti. Stabilita jednotlivých fixátorů je vyhodnocena na základě výsledků zátěžových testů provedených na ortopedických modelech pánve, při kterých byla měřena dislokace zvolených bodů na dorzálním povrchu křížové kosti. Experimentální data byla pořízena a zpracována s využitím metod fotogrammetrie a korelace obrazu. Fotogrammetrický software použitý pro analýzu byl v rámci práce detailně testován a byla určena jeho přesnost.

Klíčová slova Křížová kost, iliosakrální šroub, transilikální vnitřní fixátor, transiliakální dlahy, sakrální tyč, experimentální analýza, fotogrammetrie, korelace obrazu.

TABLE OF CONTENTS

1	Introduction	1
2	Sacrum Fixation Techniques	3
2.1	Anatomy of Pelvis	3
2.2	Pelvic Fractures	5
2.3	Fixation Techniques	8
3	Photogrammetry and Digital Image Correlation	13
3.1	Image Acquisition	14
3.2	Scene Reconstruction	14
3.3	Image Recognition and Matching	19
4	Experimental Analysis	21
4.1	Experimental Setup	21
4.2	Preliminary Tests	26
4.3	Analysis of Selected Fixators	29
4.4	Data Processing and Evaluation	31
5	Results of Comparative Study	36
5.1	Intact Models	36
5.2	Fractured Models	37
6	Conclusion	43

TABLE OF CONTENTS	vi
A Appendices - Software Tools	44
A.1 Calibration Target Analysis	44
A.2 Centre of Gravity Detection	45
References	46
List of Publications	51

LIST OF FIGURES

2.1	Pelvis. The anterior (left) and lateral (right) view.	4
2.2	Sacrum. The anterior (left) and posterior (right) surface.	5
2.3	Types of fixators	11
3.1	Pinhole camera model	14
3.2	Stochastic pattern	19
3.3	Dot pattern	19
4.1	Physiological position of the pelvis (left) and its position for loading (right).	23
4.2	Model fixed to the stand. The compressive element and the extensometer attached to the model.	23
4.3	Positioning of cameras and lights	25
4.4	Analysed points	25
4.5	Ratio of displacement of the compressive element and the point C1.	28
4.6	Data processing procedure - time synchronisation	32
4.7	Data processing procedure - applied load	32
4.8	Different progress of data obtained from extensometer. (a) No noise, (b) Creeping, (c) Insignificant noise, (d) Significant noise.	35
5.1	Force-displacement curve of the models in the intact state.	38
5.2	Force-displacement curve of the fractured models treated with given fixator.	38
5.3	Stiffness of the models in the intact state and of fractured models treated with given fixator.	39

5.4	Relative displacement of both sides of the fracture	39
5.5	Highlighted contours of fracture and sacral foramina. Unloaded state in the first cycle (left), maximal loading in the first cycle (middle), maximal loading in the last cycle (right).	41
5.5	Highlighted contours of fracture and sacral foramina. (<i>Continued</i>)	42
A.1	Chessboard - GUI	44
A.2	Centre of gravity - GUI	45

LIST OF TABLES

4.1	Material properties of pelvic model (solid foam), compared to material properties of femur and tibia. Results from tensile tests. [14, 15, 16]	22
4.2	Comparison of the DIC software and the extensometer.	26
4.3	Displacement of the compressive element (CE) and the point C1.	28
4.4	Total displacements of points C0 and C1 and their displacement in vertical direction at applied load 500 N. Table contains data recorded by extensometer (Ext.) and results from DIC analysis (DIC).	30
5.1	Stiffness of the models in intact state and at fractured models treated with given fixator.	38

1

INTRODUCTION

Pelvic injuries are not very common in comparison with fractures of other bones in human body. However, their occurrence significantly rises among polytraumatized patients and patients after motor vehicle accidents [1, 2]. A lot of attention has to be paid on these fractures as they may be very serious. When the fractures are unstable and a surgical treatment is necessary, there can be used several different types of either internal or external fixators to support the healing of bone structures.

The greatest treatment issue is the high incidence of wide range of surgical complications, such as vascular injuries, thromboembolic complications or risk of infections. These are mostly caused by improper preoperative diagnostics and inappropriately selected fixator. To minimize the risk of the difficulties mentioned above it is necessary to analyse the fracture in detail and assess the suitability of each possible stabilisation method. Therefore it is very important to know how the specific fixator behaves when it is chosen for the treatment. In order to stabilise the bone well and to shorten the process of healing, the fixator must prevent both sides of the fracture from large relative displacements. On the other hand, the fracture cannot be tighten too much so as not to produce any considerable tension in the area because of many nerves that could be damaged.

This thesis is focused on the sacral bone fractures which represent, together with the fractures of pubic bones or diastasis of pubic symphysis, the most common injuries in the pelvic region. The essential task is the experimental comparison of the stability of four widely used fixators. Nominally, the thesis compares transiliac internal fixator (TIFI), iliosacral screws (ISS), transiliac plate (TP) and sacral bars (SB). Their stability is evaluated according to the relative displacements of the both parts of the fractured bone. Basically, the lower the displacement, the more stable the fixation. Nevertheless, in the practice of medicine the situation is more complicated, as all the risks must be considered as well as the difficulties of application of given fixators. This thesis provides

the guide to selected fixators from the mechanical point of view.

The orthopaedic models of male pelvis made of solid foam are used for the experiments [12]. Using models instead of cadaveric pelvis increases the repeatability of the experiments with the same initial conditions every time. Compared to human bones which differ in their geometry, material properties and health and could be mechanically damaged, the models are almost identical. This fact is crucial for the measurements as the task is not to simulate the exact behaviour of bone but to obtain comparable results from several experiments.

A lot of studies focused on various pelvic ring fixation techniques were done, some with models or cadaveric pelvis and some which studied patients with treated sacral fracture [20]-[30]. However, most of them describe only one or compare two types of fixators. As the measurements in each study were made under different conditions, their results cannot be explicitly compared. The aim of this study is to make more extensive experimental research which brings comparable results for four fixators mentioned above.

The thesis is divided into six chapters, including the introduction and the conclusion.

The second chapter provides a description of pelvic anatomy, types of its fractures and each of the compared stabilisation methods. There are depicted the specifications of the fixators and the techniques how they are used to stabilise and treat the fracture. Previous studies focused on each fixator are mentioned there.

In the third chapter, there is the principle of the digital image correlation, which is the method used for the analysis of the graphical data obtained during the experimental measurements.

In the fourth chapter, there is a description of the experimental setup, the work flow and the method of the data analysis. The suitability of proposed experimental procedure is verified by a serie of preliminary measurements.

The fifth chapter gives the results of the comparative study of fixators. There is presented a mechanical behaviour of models stabilised by selected fixators. Afterwards, the results are compared and the stability is discussed.

SACRUM FIXATION TECHNIQUES

2

2.1 Anatomy of Pelvis

The pelvis is a bony ring located in the lower trunk. It is formed by four bones - left and right coxal bone, the sacrum and the coccyx (Fig. 2.1). The pelvis fulfils very important functions in human body - it protects abdominopelvic viscera, such as the reproductive organs and the urinary tract, and it bears the weight of the upper part of body and transfers the weight to the lower limb.

There are many structural differences between male and female pelvis, most of them are related to the female's role in pregnancy and childbirth. In comparison to the male pelvis, the female one is shorter and wider, there is greater hollow space within the ring of pelvic bones and the pubic symphysis is more flexible [4].

2.1.1 Os Coxae (coxal bone)

Ossa coxae, called also hip bones, coxal bones or innominate bones are flat irregularly shaped paired bones. They are the largest pelvic bones. In the anterior part of the pelvis they are joined to each other by the pubic symphysis - the cartilage-like, slightly movable joint. In the posterior part they are connected to the sacrum by the sacroiliac joints. These are very strong and stable and together with associated ligaments they allow just slight movements between the coxal bones and the sacrum.

The hip bones actually consist of three individual bones - the ilium, ischium and pubis. In childhood, these bones are separate, they are fused together by the end of puberty. In the place where these three bones meet they form the acetabulum, a large circular cup-like cavity which articulates with the head of the femur.

The ilium is the uppermost broad bone which forms the prominence of the hip. The ischium is the posteroinferior, strongest portion of the hip bone and the pubis is that portion which is situated between the acetabulum and the pubic symphysis.

2.1.2 Os Sacrum (sacrum)

The sacrum (Fig. 2.2) is synostosis of five sacral vertebrae at the inferior end of the spine. Analogous to the hip bones, after birth the sacrum consists of five sacral vertebrae (occasionally the number is reduced to four) that become fused in the adulthood.

Because of its shape the sacrum belongs to the group of irregular bones [3]. From the anterior view it is approximately triangular. From the lateral view it is concave, broad above and narrow in the lower end. Its upper base is articulating with the fifth lumbar vertebra (L5), its apex is articulating with the coccyx.

The sacral surface differs significantly on its anterior and posterior part. The anterior surface is smooth and concave in both vertical and horizontal direction. In the middle there are visible transverse ridges which indicate of the original division into separate vertebrae. At each end of the ridges there are paired holes, called the sacral foramina. The posterior surface is rugged and is flatter in the vertical direction than the anterior one. In the central line there is the median sacral crest with three or four tubercles.

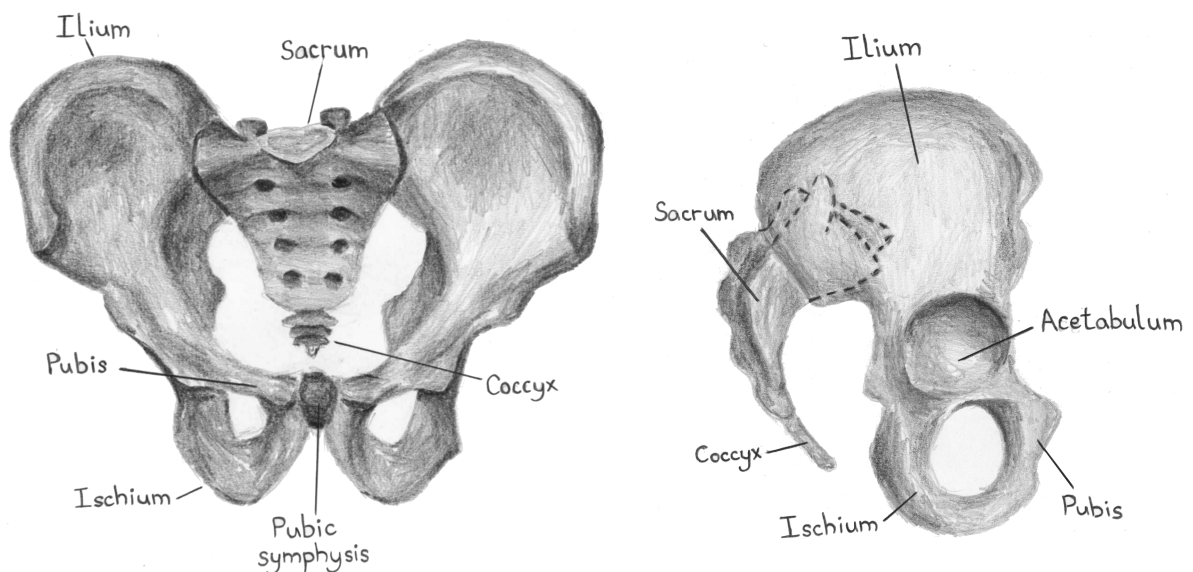


Fig. 2.1: Pelvis. The anterior (left) and lateral (right) view.

Throughout the greater part of the bone runs the sacral canal. It lodges the sacral nerves which pass out through the sacral foramina.

2.1.3 Os Coccygis (coccyx)

The coccyx is a triangular bone usually formed of four or five fused coccygeal vertebrae. It is very thin from the lateral view. Its anterior surface is concave with three visible grooves marking the junction of the vertebrae. The posterior convex surface is also marked by those grooves. Both the sacrum and the coccyx consist mostly of the trabecular bone covered by a thin layer of a compact bone.

2.2 Pelvic Fractures

Fractures in the pelvic region are rare. They hardly ever occur as the only injury; mostly they are accompanied by chest injuries, long bone fractures, head and abdominal injury or spine injury [9]. The incidence of this kind of injury is generally associated with the high-energy trauma, such as that generated in motor vehicle accidents or falls from great heights [7]. The most endangered groups in population are young people involved in sports and elderly people suffering from osteoporosis [1].

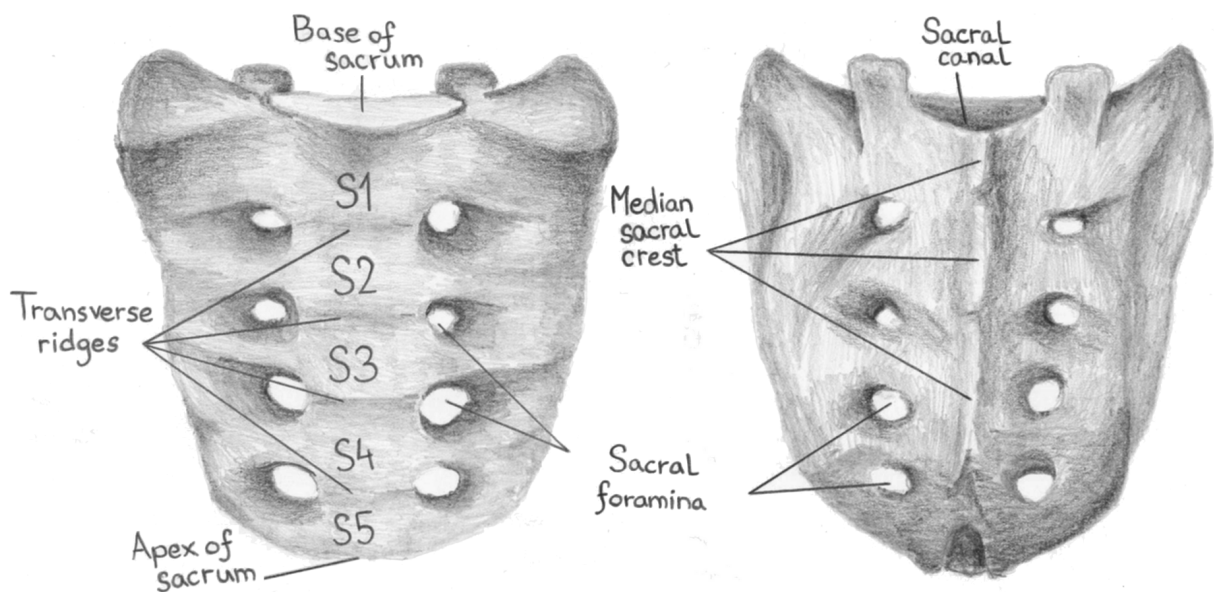


Fig. 2.2: Sacrum. The anterior (left) and posterior (right) surface.

In spite of quite low occurrence of pelvic fractures, a lot of attention is paid to it because of its seriousness. The greatest problem associated with these injuries is that there are many nerves, blood vessels and viscera in the pelvic region and therefore the injuries can seriously endanger patient's health or even their life. Contrary to the progress in treatment, the unstable pelvic fractures still have a high acute mortality and may cause severe late sequelae [10].

As there can occur a great variety of fractures in the pelvic region, a classification is important to describe their nature. First classification system for the pelvic fractures was introduced by the French surgeon Joseph François Malgaigne in the beginning of the 19th century. Since that time more than fifty classification systems have been created. Some of them have just descriptive nature whilst the other provide clinically relevant classification based on the mechanism of the injury.

2.2.1 Marvin Tile's Classification

According to Marvin Tile's classification [7], the injuries can be divided into three groups, using the pelvic ring stability as the dividing criterion.

A-type: Stable pelvic ring injuries

Stable fractures, mostly caused by low-energy trauma, are those which does not affect the stability of the pelvic ring. These injuries can be further divided into following categories:

- A1 - avulsion of the hip bone,
- A2 - stable iliac wing fracture or stable, minimally displaced pelvic ring fracture,
- A3 - transverse sacral or coccygeal fracture.

B-type: Partially stable pelvic injuries

Disruptions classified as the B type injuries are rotationally unstable whilst the vertical stability is not affected. They are characterised by a complete disjunction in pubic symphysis region combined with partial disruption in the posterior part. Among B-type injuries belong these fractures:

- B1 - symphyseal diastasis with partial sacroiliac diastasis or a sacral fracture; this type of injury is induced by an anterior-posterior compression,
- B2 - internal rotation of the hemipelvis with the pubic rami fractures and sacral fracture across the sacroiliac joint; this injury is induced by a lateral compression,
- B3 - combined bilateral B-type injuries.

C-type: Completely unstable pelvic ring injuries

The most serious fractures with the highest mortality rate are those belonging to C-type injuries. Both the rotational and the vertical stability is affected as the anterior and posterior pelvic rings are completely disrupted and the hemipelves are vertically displaced. Subgroups of injuries of this type are following:

- C1 - unilateral C-type injury,
- C2 - unilateral C-type injury, contralateral B type injury,
- C3 - bilateral C-type injuries.

This classification served as a template for the AO/OTA classification which is currently used [17]. Both of them are almost identical - in both cases, M. Tile was their lead author. In AO/OTA classification, pelvic fractures are identified by number 61 followed by specification letter and number mentioned above.

2.2.2 Denis Three-zone Classification System of Vertical Sacral Fractures

Denis classification categorizes vertical fractures of the sacrum according to the location of the fracture in relation to the sacral foramina [7]:

- **Type I: transalar;** the fracture is lateral to the sacral foramina, nervous structures are usually not affected,
- **Type II: transforaminal;** the fracture line runs through the sacral foramina, it is associated with the lesion of sacral nerve roots in approximately 25 % of cases,
- **Type III: central;** the fracture line is medial to the sacral foramina, involving the spinal canal; more than 50 % of these fractures are associated with neurological injuries.

2.3 Fixation Techniques

This thesis is focused on the Denis Type II fracture which may be a part of C1 fracture according to Marvin Tile's classification, eventually 61-C1.3 according to AO/OTA classification [18].

There exist many fixation techniques for the pelvic fracture stabilisation in the medical practice. The suitability of each kind differs from patient to patient according to the nature of fracture, the accompanied injuries and the overall patient's health state. There are also differences in popularity of specific fixators around the world, based on local experience and habits.

Types of fixators examined in this study were selected in close cooperation with the Department of Orthopaedics and Traumatology, Faculty of Medicine of Charles University and Faculty Hospital in Pilsen, Czech Republic. Each of these four fixators belongs to the group of minimally invasive fixation techniques. Contrary to the open techniques widely used in the past, these allow for the stabilisation with significantly less damage of surrounding tissues whilst providing adequate treatment possibilities in the most of cases [8].

2.3.1 Transiliac Internal Fixator

The transiliac internal fixator (TIFI) consists of two polyaxial screws inserted in the alae of the ilium that are transfixed with a connection rod, forming together an angular stable construction (Fig. 2.3a). This technique is quick and minimally invasive and minimizes damage to surrounding tissues.

This stabilisation technique is suitable for

- unilateral sacral fractures,
- unilateral dislocations in sacroiliac joint.

Conversely, it cannot be used in following cases:

- fractures of ala of the ilium which makes the screw insertion impossible,
- bilateral sacral fractures when no other fixator is applied, such as iliosacral screw or spinopelvic fixation,
- serious injuries of gluteal soft tissues,

- open fractures,
- injuries with neurological deficit.

The first study describing operative technique for TIFI and its clinical results was made by Füchtmeier et al. in 2004 [31]. In 2011 Dienstknecht et al. evaluated its biomechanical characteristics and compared the stability of TIFI to that of iliosacral screws and ventral plate osteosynthesis [23]. According to their study, performed on cadaveric freshly frozen pelvises, there were no significant differences in displacements tolerated by these methods. In another study published in the same year, Dienstknecht et al. evaluated clinical results of patients who had the dorsal pelvic ring injuries stabilised by TIFI [22]. Their observations suggest TIFI is a good alternative to other established fixators.

2.3.2 Iliosacral Screws

The iliosacral screws (ISS) are commonly used type of pelvic fixator (Fig. 2.3b). However, their application is difficult and many complications may be associated to it [24]. Some of the complications are caused by improper screw insertion, the other by poor bone quality.

During surgery, ISS is inserted through the ala of ilium into the first or second sacral vertebra. In most of the cases, two screws are used in order to provide better rotational stability.

To minimize the risk of technical complications, the screws must be inserted precisely so as to be placed in the "safe zone" which is unique to each person. The "safe zones" are located in the first (S1) and the second (S2) sacral vertebra. However, screws are inserted into S2 only under special circumstances as the size of the "safe zone" there is smaller and the vertebra is situated more posteriorly than the first one. The zones are often located using radiography or tomography. Furthermore, modern approach to stabilisation uses navigational templates produced by 3D modelling [29].

When stabilising dorsal pelvic injuries, ISS are suitable for

- vertical sacral fractures (especially Denis type I; Denis type II and III are acceptable on condition that there is no comminutive zone in the fractured area),
- sacroiliac joint injuries.

ISS are very frequently discussed fixation technique. However, in some studies, ISS are used as the referential fixator to which the fixator of interest is compared. As mentioned

above, Dienstkecht et al. in 2011 compared TIFI to ISS and ventral plate osteosynthesis [23]. In 1999 Probe gave an overview of techniques for pelvic ring injuries [30]. ISS are mentioned there as the most common method for posterior open reduction. A method for the insertion of ISS is described in this study. Routt et al. in 1997 discussed potential complications and risks associated with using ISS, such as damage of local nerves and vascular structures and the fixation failure [24].

2.3.3 Transiliac Plate

The transiliac plate (TP) is a metal plate with holes for the insertion of screws (Fig. 2.3c). It is bent on both ends according to the shape of pelvis and then it is placed along the posterior lateral ilium and fixed to the alae of the ilium by screws on both sides. Using up to three screws on each side can achieve effective fixation [28].

TP may be used for stabilisation of following injuries

- sacroiliac joint injuries,
- sacral bone injuries without neurological deficit,
- some kinds of fractures of ala of ilium.

Contraindications to the use of TP are

- transversal sacral fractures,
- injuries accompanied by neurovascular deficit,
- comminuted fractures of ala of ilium.

As by using TIFI, there is low risk of neurovascular injury when using TP for stabilisation. Its disadvantage is higher cost and potential hypodermic irritation. Another problem is the process of bending as it cannot be performed more than once and it is very challenging to do it precisely due to irregular shape of iliac bones.

TP as a method for the stabilisation of unstable pelvic ring fractures and a technique of its application was firstly described by Albert et al. in 1993 [27]. Study of patients with unstable pelvic ring injuries treated with TP and ISS performed by Chen et al. in 2012 compares these two techniques [25]. Their results imply that both fixators have similar clinical effect but the plate has lower risk of damaging nerves and blood vessels. On the other hand, using ISS leads to lower blood loss and smaller size of required incision. In 2011 Kobbe et al. performed analysis of patients with a dorsal pelvic ring injuries treated

with TP. They recommend transiliac locked compression plate as a good alternative to ISS because its application is quick, safe and associated with a good functional outcome [20].

2.3.4 Sacral Bars

Sacral bar (SB), called also transiliac bar or sacral rod is a metal continuously threaded rod (Fig. 2.3d). In literature, the term sacral bar may refer either to a bar applied under each other through the alae of the ilium in the height of sacral base or to a bar applied through S1 vertebra. In this study, the first mentioned technique is used.

In order to provide sufficient rotational stability, two sacral bars are applied next to each other.

This technique is not very common as it was not proven to be stable and it may cause complications such as pain in the area of fixation or possible risk of extensive compression along the fracture. It is suitable only for following injuries:

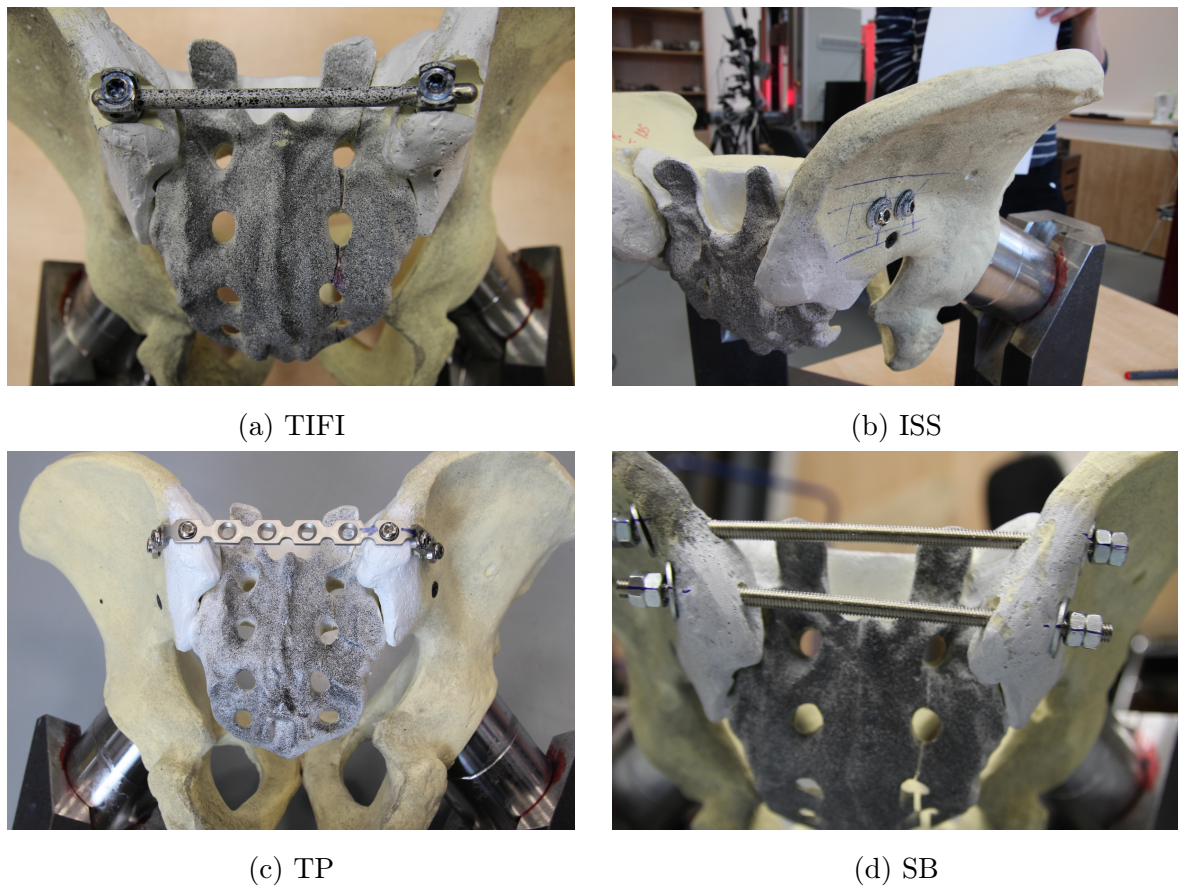


Fig. 2.3: Types of fixators

- unilateral sacral fractures without neurological deficit,
- unilateral injuries of sacroiliac joint.

In case of bilateral fracture, SB can be applied only together with another fixator such as ISS.

Probe in 1999 described the use and operative technique of SB [30]. In 1996 Gorczyca et al. compared the strength of ISS and SB. Their study performed on cadaveric pelves came to conclusion that the strength of ISS fixation was approximately 77 % of that of SB [26].

PHOTOGRAMMETRY AND DIGITAL IMAGE CORRELATION

3

In the field of measurements of displacements, deformations, strains and stresses of mechanical objects, non invasive optical techniques can be utilised. Two of them - photogrammetry and digital image correlation (DIC) - are described below.

Generally, the term DIC may refer to any correlation between images. In the field of mechanics and optics it is widely used for a class of methods measuring strain and displacements from images captured during experimental measurements [32]. According to Michael A. Sutton et al., DIC "refers to the class of non-contacting methods that acquire images of an object, store images in digital form and perform image analysis to extract full-field shape, deformation and/or motion measurements" [36].

The term photogrammetry is quite often associated with the mapping of the surface of the earth using aerial photographs and producing maps. However, it is also used in astronomy, medicine, crime detection and accidents investigation [33]. According to Oxford Dictionaries, photogrammetry is "the use of photography in surveying and mapping to ascertain measurements between objects" [34]. Collins English Dictionary describes it as "the process of making measurements from photographs, used esp in the construction of maps from aerial photographs and also in military intelligence, medical and industrial research, etc." [35].

In principle, both terms can refer to the same process.

Briefly, the whole process of making measurements using images consists of three major parts. In one part 2D images of examined object are recorded. Photographic pictures are used most often, however, in some fields such as cartography there can be used radars or other scanning devices. Other part is focused on image recognition and matching. The main part deals with spatial reconstruction of the object. Each part of the process is described below.

3.1 Image Acquisition

Three dimensional object can be mapped on two dimensional image by using a camera. Digital camera is an opto-electronic system consisting of optics, hardware and the digitization and storage process. When using digital camera, the captured image is stored as an array of discrete digital intensity data.

In the pinhole camera model, which is the simplest model, there is an image plane and a centre of projection C that lies on the optical axis o (Fig. 3.1). A point in the captured scene is mapped on the image plane if it is situated in the field of view of the camera, that means if a ray leading from the point through the centre of projection intersects the image plane. If so, this intersection represents the image of the point [36].

When a 3D world is projected onto a 2D plane, there is a loss of one dimension. Due to this loss, all the points that lie on the same ray leading through the centre of projection are projected onto the same location on the image plane. When the examined object is planar and it is not perpendicular to the image plane, using only one camera is sufficient for its reconstruction. In all other cases, at least two cameras capturing the object from different angles are necessary so as to obtain relevant spatial information.

3.2 Scene Reconstruction

Scene reconstruction is a process when the spatial coordinates of the object are determined based on their coordinates in 2D images. Prior to the reconstruction, camera calibration

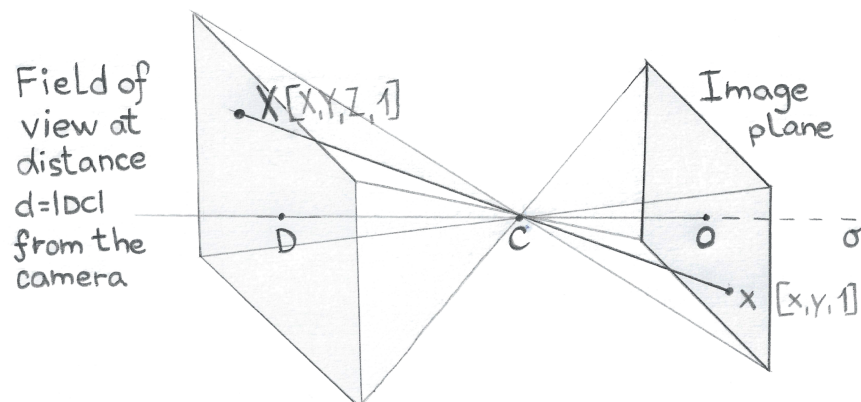


Fig. 3.1: Pinhole camera model

which determines parameters of cameras and their spatial orientation with respect to given point is necessary.

When assuming that the mapping between camera and real world is linear, the Direct Linear Transformation (DLT) method [37] can be utilised for the camera calibration. Its principle is explained below for one and two cameras and then it is generalised for arbitrary number of cameras.

In the following homogeneous coordinates are used to describe location of points [37]. In the three-dimensional Euclidean space, having the origin in the centre of projection \mathbf{C} , a point \mathbf{X} is represented by an ordered triple of real numbers, $\mathbf{X} = [X, Y, Z]$. In the field of image processing, it is convenient to use homogeneous coordinates. The main reason why these are used is that they can capture the concept of infinity which does not exist in Euclidean space.

Homogeneous coordinates are generated from inhomogeneous by adding one extra coordinate. Thus, in homogeneous coordinates is $\mathbf{X} = [X, Y, Z, 1]$. The last coordinate is called the scale. Points expressed using homogeneous coordinates are said to be equivalent when they differ by a common multiple k . Multiplication of the homogeneous coordinates by the scale, $[X, Y, Z, 1] = k[X, Y, Z, 1] = [kX, kY, kZ, k]$ does not affect the original inhomogeneous ones as they can be obtained by dividing by k and removing the last extra coordinate.

As mentioned above, all points can be expressed using arbitrary non-zero scale. However, none of them corresponds to point with coordinates $[X, Y, Z, 0]$. When divided by 0, the coordinates $[X/0, Y/0, Z/0]$ refer to infinity. Therefore, points at infinity are defined by using zero as the extra coordinate.

3.2.1 Single View Projection

As described above, using a single camera is sufficient for measurements of planar objects. To determine the properties of camera (i.e. the transformation between real world and the image), a photo of calibration object situated in the analysed plane must be taken. This object, called the calibration target, has on its surface given number of points with known coordinates.

Homogeneous coordinates of n points of the calibration target in the world coordinate system are $\mathbf{X}_i = [X_i, Y_i, W_i]^T$ where $i = 1, 2, \dots, n$ is a number of the point. Their

projections on the acquired image have homogeneous coordinates $\mathbf{x}_i = [x_i, y_i, w_i]^T$ in the image coordinate system. When there is a sufficient number of point correspondences $\mathbf{X}_i \leftrightarrow \mathbf{x}_i$, camera matrix \mathbf{P} can be computed.

Image coordinates \mathbf{x}_i must satisfy following equation

$$\mathbf{x}_i = \mathbf{P}\mathbf{X}_i, \quad \mathbf{i} = 1, 2, \dots, n, \quad (3.1)$$

In this case, \mathbf{P} is 3×3 matrix. Multiplying the equation by \mathbf{x}_i produces

$$\mathbf{N} = \mathbf{x}_i \times \mathbf{P}\mathbf{X}_i, \quad (3.2)$$

where $\mathbf{N} = [0, 0, 0]^T$. Rewriting

$$\mathbf{P} = \begin{bmatrix} \mathbf{p}_1 \\ \mathbf{p}_2 \\ \mathbf{p}_3 \end{bmatrix}, \quad (3.3)$$

where \mathbf{p}_i are rows of \mathbf{P} matrix, the following set of equations is obtained

$$\underbrace{\begin{bmatrix} \mathbf{N}^T & -w_i\mathbf{X}_i^T & y_i\mathbf{X}_i^T \\ w_i\mathbf{X}_i^T & \mathbf{N}^T & -x_i\mathbf{X}_i^T \\ -y_i\mathbf{X}_i^T & x_i\mathbf{X}_i^T & \mathbf{N}^T \end{bmatrix}}_{\mathbf{A}_i} \underbrace{\begin{bmatrix} \mathbf{p}_1^T \\ \mathbf{p}_2^T \\ \mathbf{p}_3^T \end{bmatrix}}_{\mathbf{p}} = \mathbf{N}, \quad (3.4)$$

where \mathbf{A}_i is a 3×9 matrix and \mathbf{p} is 9×1 matrix containing transposed rows of matrix \mathbf{P} . The matrix \mathbf{A}_i has a rank 2 as only two of its rows are linearly independent. The third line is usually omitted and so the size of \mathbf{A} is 2×9 . The set of equations (3.4) is transformed into

$$\underbrace{\begin{bmatrix} \mathbf{N}^T & -w_i\mathbf{X}_i^T & y_i\mathbf{X}_i^T \\ w_i\mathbf{X}_i^T & \mathbf{N}^T & -x_i\mathbf{X}_i^T \end{bmatrix}}_{\mathbf{A}_i} \mathbf{p} = \mathbf{N}, \quad (3.5)$$

The \mathbf{p} matrix has 9 elements, however, it is defined up to scale [37] and thus it has only 8 degrees of freedom. Therefore, at least 4 points are necessary to solve this set of equations. The matrices \mathbf{A}_i form together matrix $\mathbf{A} = [\mathbf{A}_1^T \mathbf{A}_2^T \dots \mathbf{A}_n^T]^T$ with size $2n \times 9$. The set of equations for all points has form

$$\mathbf{A}\mathbf{p} = \mathbf{N}. \quad (3.6)$$

In an ideal case when the coordinates of points in the image are exact, using 4 or any higher number of points leads to exact solution of the set of equations as the rank

of the *A* is always equal to 8 [37]. In real images with noise and accuracy limited by image resolution, using more than 4 points is desirable. In this case the exact solution does not exist and algebraic methods are used to find an approximate solution of \mathbf{p} matrix by minimising $\|\mathbf{A}\mathbf{p}\|$ [37].

When the \mathbf{p} matrix is computed and its elements are put into the \mathbf{P} matrix, it is possible to compute real-world coordinates of any point based on its image coordinates using equation (3.1).

3.2.2 Two View Projection

When the object to be analysed is three-dimensional, at least two cameras are necessary for its 3D reconstruction. The principle of the 3D analysis is derived from the 2D algorithm described above.

The point \mathbf{X}_i of the calibration target has coordinates $\mathbf{X}_i = [X_i, Y_i, Z_i, W_i]$ in the world coordinate system. Its image on the image plane of the first camera has coordinates $\mathbf{x}_{1i} = [x_{1i}, y_{1i}, w_{1i}]$ in the image coordinate system. On the image plane of the second camera the image of the point \mathbf{X}_i has coordinates $\mathbf{x}_{2i} = [x_{2i}, y_{2i}, w_{2i}]$. For both cameras their camera matrices \mathbf{P}_1 and \mathbf{P}_2 are computed using equation (3.1)

$$\mathbf{x}_{ji} = \mathbf{P}_j \mathbf{X}_i, \quad j = 1, 2, \quad i = 1, 2, \dots, n, \quad (3.7)$$

where j is a number of the camera. In this case, the size of matrices \mathbf{P}_1 and \mathbf{P}_2 is 3×4 .

The set of equations (3.6) is solved for both cameras

$$\mathbf{A}_j \mathbf{p}_j = \mathbf{N}. \quad (3.8)$$

The equations (3.6) and (3.8) are formally identical, they differ in the size of matrices, where in the case of 3D, $\mathbf{N} = [0, 0, 0, 0]^T$, size of \mathbf{A}_j is $2n \times 12$ and size of \mathbf{p}_j is 12×1 . Matrix \mathbf{p}_j has 11 degrees of freedom and so at least 6 points are required for the reconstruction.

Spatial coordinates of any point \mathbf{X}' with its projections $\mathbf{x}'_1 = [x_1, y_1, w_1]$ on the image plane of the first camera and $\mathbf{x}'_2 = [x_2, y_2, w_2]$ on the image plane of the second camera can be obtained from

$$\mathbf{N} = \mathbf{x}'_j \times \mathbf{P}_j \mathbf{X}'. \quad (3.9)$$

This can be rewritten in the form

$$\underbrace{\begin{bmatrix} y_1\mathbf{P}_{13} - w_1\mathbf{P}_{12} \\ w_1\mathbf{P}_{11} - x_1\mathbf{P}_{13} \\ x_1\mathbf{P}_{12} - y_1\mathbf{P}_{11} \\ y_2\mathbf{P}_{23} - w_2\mathbf{P}_{22} \\ w_2\mathbf{P}_{21} - x_2\mathbf{P}_{23} \\ x_2\mathbf{P}_{22} - y_2\mathbf{P}_{21} \end{bmatrix}}_{\mathbf{B}} \mathbf{X}' = \mathbf{N}, \quad (3.10)$$

where the first triple of rows of \mathbf{B} matrix contains data from the first camera, the second triple contains data from the second camera. Solving this set of equations, spatial coordinates of point \mathbf{X}' are obtained. The third (respectively the sixth) line is the linear combination of the first and the second (respectively the fourth and the fifth) line. Therefore, they can be omitted and the form of \mathbf{B} matrix is

$$\mathbf{B} = \begin{bmatrix} y_1\mathbf{P}_{13} - w_1\mathbf{P}_{12} \\ w_1\mathbf{P}_{11} - x_1\mathbf{P}_{13} \\ y_2\mathbf{P}_{23} - w_2\mathbf{P}_{22} \\ w_2\mathbf{P}_{21} - x_2\mathbf{P}_{23} \end{bmatrix}. \quad (3.11)$$

3.2.3 Generalised Multiple View Projection

When using more than two cameras for the scene reconstruction, the equations are the same as when using two cameras. The only difference is the size of matrix \mathbf{B} which is $2c \times 4$ where c is number of cameras

$$\mathbf{B} = \begin{bmatrix} y_1\mathbf{P}_{13} - w_1\mathbf{P}_{12} \\ w_1\mathbf{P}_{11} - x_1\mathbf{P}_{13} \\ y_2\mathbf{P}_{23} - w_2\mathbf{P}_{22} \\ w_2\mathbf{P}_{21} - x_2\mathbf{P}_{23} \\ \vdots \\ y_c\mathbf{P}_{c3} - w_c\mathbf{P}_{c2} \\ w_c\mathbf{P}_{c1} - x_c\mathbf{P}_{c3} \end{bmatrix}. \quad (3.12)$$

All the equations presented above are valid if an ideal optics (pinhole camera model) is considered. When using real optics, the image is distorted and nonlinear transformation must be utilised [37].

3.3 Image Recognition and Matching

So as to perform the scene reconstruction, analysis of the images is necessary. An algorithm can be used to detect the objects and to set the correspondences between images.

First correlation process takes its course when the cameras are calibrated and photos of calibration target are analysed. Commonly used calibration targets have either chessboard pattern or a dot grid. Chessboard calibration target will be considered in this text. It has specified number of squares with specified size. Corners of the squares are usually used as the identifying points. Set of data containing the coordinates of the corners in the world coordinate system and coordinates of their projections on all image planes in the image coordinate systems is used as the input data for the reconstruction algorithm. A software tool developed by the author which performs the analysis of the calibration target is described in Appendix A.1.

If the whole surface of the object is to be analysed, an option how to perform the analysis is the application of stochastic pattern on the object (Fig. 3.2). Analysis of the surface based on single pixels is impossible as there are many pixels with the same gray value in the image. Therefore, a squared area called facet with given size in pixels. The whole object in the image is divided into the squares that are to be identified in other images. The correlating algorithm must consider that due to different position of cameras, the pattern is deformed and can be distorted in other images and its gray values can differ slightly.

If just a set of discrete points on the surface of the object are analysed instead of the

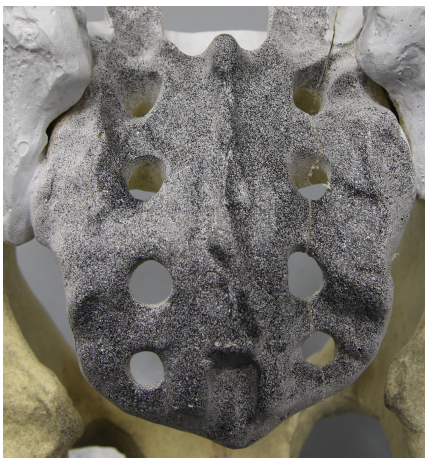


Fig. 3.2: Stochastic pattern

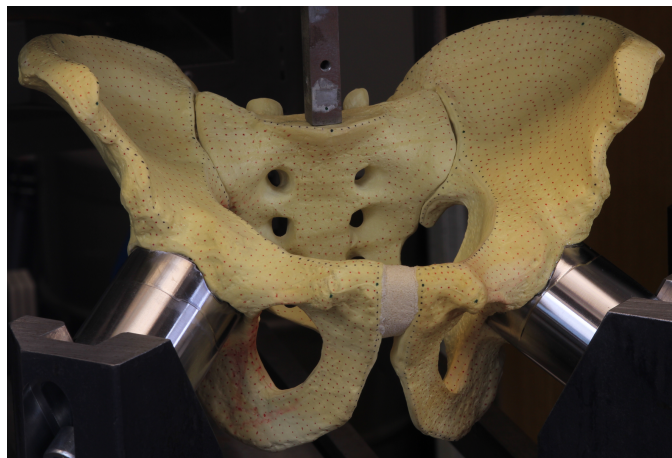


Fig. 3.3: Dot pattern

stochastic pattern covering the entire surface of the object, the process of image matching can be performed manually by identifying unique points on the object or by applying a specific pattern such as dots (Fig. 3.3). The software tool developed by the author which is applicable for semi-automatic correlation of images from two cameras and fully automatic correlation between a serie of images is presented in Appendix A.2.

EXPERIMENTAL ANALYSIS

4.1 Experimental Setup

4.1.1 Pelvic Models

For the experiments, solid-foam male pelvic models were utilised [12]. Bone models made of solid foam are used by orthopaedists for practicing surgeries, especially application of external and internal fixations. Models used in this study have pubic symphysis made of soft sponge-like material and rigid sacroiliac joints - the sacrum and the ilium are joined together by glue and screwed to each other.

Material properties

The material of the model is considered to be homogeneous and isotropic. Its properties were identified based on tensile tests performed at NTIS - New Technologies for the Information Society research centre [13]. The following material properties were identified:

- Young's modulus $E = 0.18$ GPa,
- tensile strength $R_m = 4.1$ MPa,
- Poisson's ratio $\nu = 0.2$,
- density $\rho = 280$ kg·m⁻³.

In tab. 4.1 material properties of solid foam are compared to those of real trabecular and compact bones - femur and tibia - based on results of tensile tests. According to these data, the Young's modulus of the model's material is 60-70 % less than that of trabecular bone and its tensile strength is approximately 25-40 % less than the tensile strength of

trabecular bone. Both the Young's modulus and the tensile strength of compact bone are significantly higher than those of the solid foam.

However, material properties of particular bones cannot be determined exactly as they vary significantly in population and they are influenced by many factors, such as the age, gender, physical condition and genetic predisposition of given person. This variety can be illustrated by results of study performed by Martens et al. [16]. They tested femoral trabecular bones of six cadavers, while several specimens were taken from each of them. Young's modulus of specimens of 56 years old male was 84 ± 89 MPa whilst Young's modulus of specimens of 32 years old female was 2024 ± 1113 MPa. Thus an application of model made of solid foam with given material properties within this comparative study is advantageous.

Preparation of the model for the measurements

For the mounting of the model, a special stand made of steel was designed and manufactured. It enabled fixing of the pelvis in the hip joints. Based on Young's modulus of solid foam, Young's modulus of steel and applied loads, the steel stand was considered to be rigid. There were the artificial femoral heads on the stand which were manufactured based on the 3D scan as the exact negative copy of the model's acetabula. They provided stable support for the model. The pelvic model was mounted to the stand by using a 2-component cyanoacrylate glue.

In the physiological position there is approximately 45° angle between the sacral base and the horizontal plane [11]. So as to provide optimal conditions for the measurements

Tab. 4.1: Material properties of pelvic model (solid foam), compared to material properties of femur and tibia. Results from tensile tests. [14, 15, 16]

	Young's modulus [GPa]	Tensile strength [MPa]
Solid foam	0.180 ± 0.017	4.1 ± 0.3
Femur - compact bone	11.4–19.7	107–140
Tibia - compact bone	20.90 ± 3.26	228 ± 31
Femur (proximal)- trabecular bone	0.616 ± 0.707	6.6 ± 6.3
Tibia (proximal) - trabecular bone	0.445 ± 0.257	5.3 ± 2.9

described below, the pelvic model was positioned in the way that the base of sacrum was horizontal (Fig. 4.1). During the positioning, attention was paid to minimisation of the prestress in the model.

A black and white stochastic speckle pattern was sprayed on the area of interest, in this case it was the dorsal surface of the sacrum. This step was necessary for the experimental data evaluation by using software for digital image correlation (DIC) described below.

Although all the models should have been absolutely identical, there were obvious little distinctions. Therefore, a serie of measurements was performed on the intact model. The measurements were supposed to identify eventual differences between the models.

Once all the measurements of the intact model were done, the sacral fracture was surgically created and the given fixator was applied by the orthopaedist.

This study examined Denis type II fracture. In the majority of cases this fracture is accompanied by a disjunction in pubic symphysis region which produce together the C1-type fracture. As this study did not examine the fixation techniques used for the anterior pelvic injuries, that area was left intact and only the sacral fracture was created. This approach eliminates the influence of the reliability of fixation in the pubic symphysis region and allows attention to be focused on sacral fracture fixations.

4.1.2 Experimental Testing Device

During the experiment, the model was repetitively loaded in compression. The machine used for the loading was the tensile testing machine ZWICK/ROELL Z050. The load

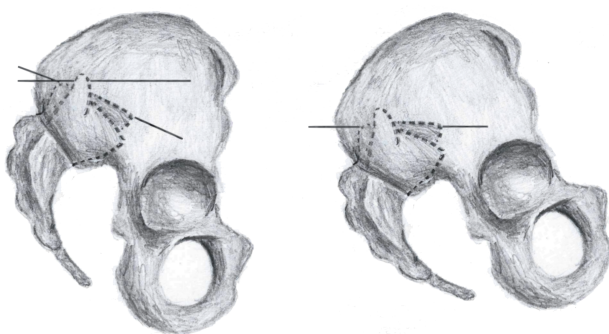


Fig. 4.1: Physiological position of the pelvis (left) and its position for loading (right).

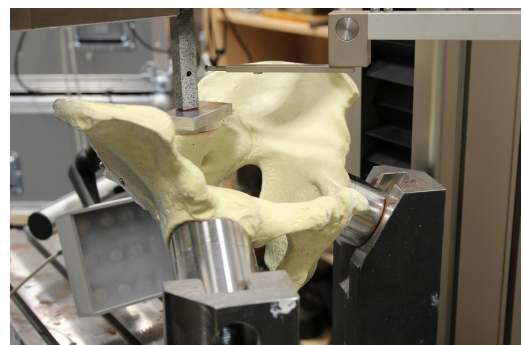


Fig. 4.2: Model fixed to the stand. The compressive element and the extensometer attached to the model.

was applied via a cuboidal compressive element and its displacement was measured by attached extensometer (Fig. 4.2). Considering the equipment of laboratory, load cell suitable for loading up to 50 kN was used. As the model was loaded with maximal force 0.5 kN, which represented 1 % of the range of the load cell, the performed measurements are at the edge of reliability of the applied device.

A set of data was obtained from the testing machine, including following information:

- prescribed shifts of the compressive element,
- real shifts of the compressive element measured by the extensometer,
- load force,
- voltage,
- acquisition time.

The data were recorded at frequency 100 Hz.

The data for analysis of displacements were obtained and executed by using the commercial software package ISTR4 4D that enables DIC analysis using multicamera system (the DIC software) [19]. Prosilica GT2300 cameras that enable a sensor resolution up to 4 Mpx at 29 Hz in grayscale were used for the image acquisition during the experiment. The frame frequency was set to 0.1 Hz.

There were four cameras placed on a vertical mounting bar in front of the model (Fig. 4.3). The scene was uniformly illuminated using two sources of red LED light in order to increase contrast of the grayscale images.

4.1.3 Data Acquisition

The DIC software and the testing machine were synchronised using a TTL signal - a signal was sent from the DIC software to the testing machine when the image acquisition started, which enabled the detection of the moments when the digital images were recorded.

Coordinates and displacements of several points along the fracture and on the median sacral crest (Fig. 4.4) were exported from the DIC software and further analysed using in-house software tools developed by the author in the Matlab environment.

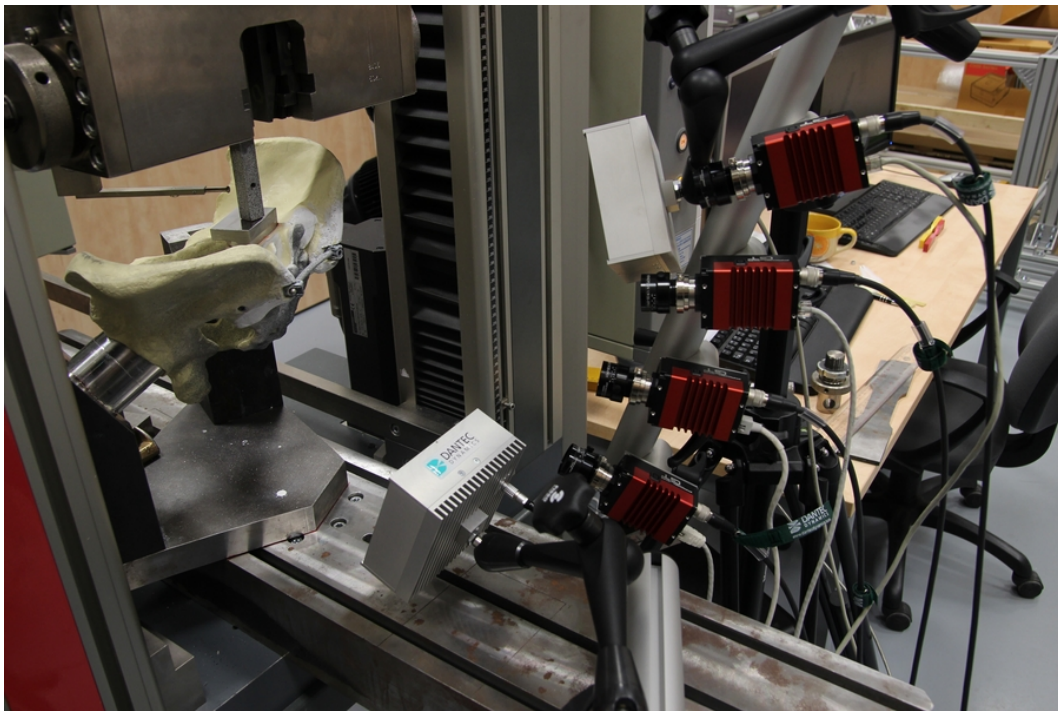


Fig. 4.3: Positioning of cameras and lights

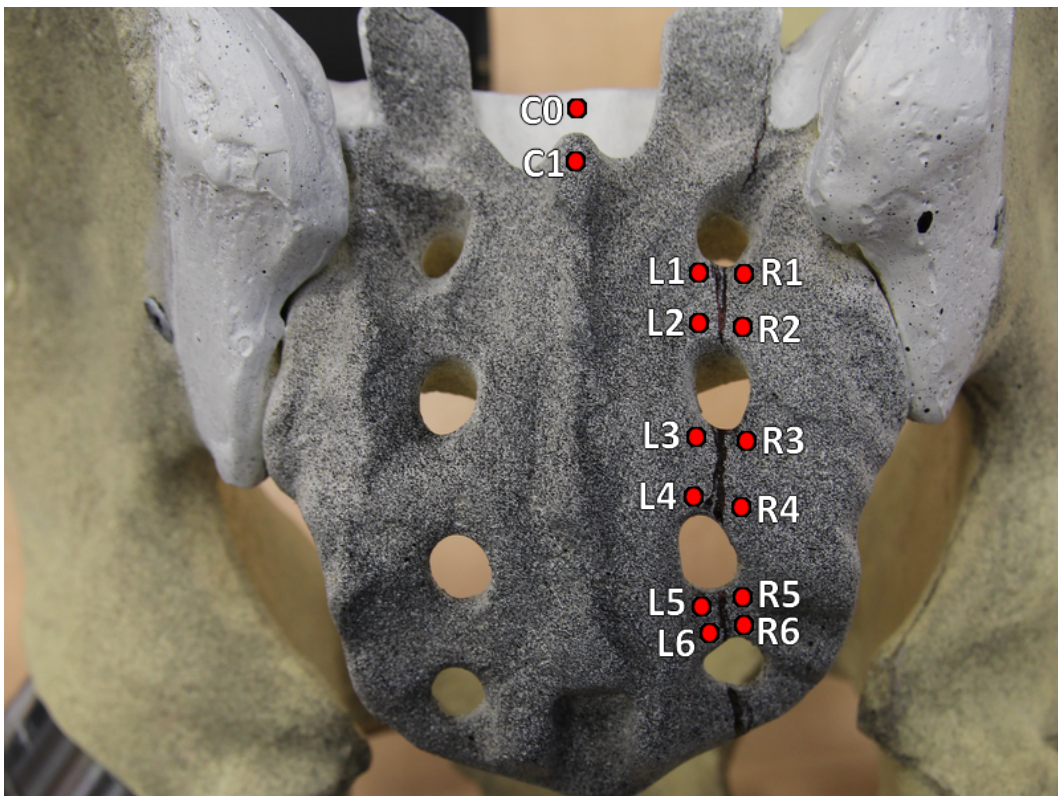


Fig. 4.4: Analysed points

4.2 Preliminary Tests

The set of measurements performed on pelvic models was one of the first measurements to be analysed by the DIC software. So as to test the software and its accuracy, a serie of preliminary experiments was made. They were used to assess the DIC accuracy and the mechanical response of the model.

4.2.1 Accuracy of the DIC Software

In order to verify the reliability of results obtained from the DIC software, a serie of tests was performed. A rigid body - metal compressive element was shifted in vertical direction and its displacement was measured by the attached extensometer. The speed of movement of the compressive element was 0.05 mm per second. Total displacement was 3 mm and the DIC images were taken at each 0.25 mm step.. The test was repeated three times.

Values of selected displacements measured by the extensometer and the DIC software are given in tab. 4.2. In all cases, the difference between results from the two devices is less than 1 %.

Tab. 4.2: Comparison of the DIC software and the extensometer.

Meas.	Prescribed displacement [mm]	Extensometer [mm]	DIC [mm]	Ratio DIC/Ext.
1	1	0.9998	1.0056	1.0058
	2	1.9997	2.0153	1.0078
	3	3.0001	3.0229	1.0076
2	1	0.9999	1.0045	1.0046
	2	1.9998	2.0112	1.0057
	3	2.9996	3.0167	1.0057
3	1	0.9993	1.0043	1.0050
	2	1.9998	2.0116	1.0059
	3	2.9999	3.0157	1.0053

4.2.2 Response of the Model to the Applied Load

In following serie of measurements, the displacement of the compressive element measured by the extensometer was compared to that of the point C1 at the median sacral crest of sacral bone (Fig. 4.4) measured by the DIC software:

- three measurements of the model treated with ISS loaded up to 500 N with 100 N steps,
- three measurements of the model treated with TIFI loaded up to 500 N with 100 N steps.

The data listed in tab. 4.3 show that the higher the applied load was, the more similar displacements of the point C1 to those of the compressive element were measured. The growth of the ratio of displacement of the point C1 to the displacement of the compressive element with the growing magnitude of applied load is depicted in fig. 4.5. This effect was caused by the loading method as the compressive element with small cross-sectional area was used. Furthermore, the surface of the sacral base was not flat and smooth, there were little variations in its elevation. Cross-sectional area of the compressive element was 2.25 cm^2 . When the measurement started, it is likely that the contact area between the compressive element and the sacral base was even smaller due to the irregular surface of the sacral base. This caused high local pressure loads at the beginning of the measurement and the compressive element flattened the surface. Consequently the load spread over larger area which decreased the local pressure peaks.

In the measurements performed for the comparative study, steel plate copying the surface of the sacral base was put between the model and the compressive element so as to improve the application of the force. As low resolution pelvic models were used, their surfaces were not identical and so the steel plate did not match all the models perfectly.

The displacements of the compressive element measured by the extensometer and the displacement of the point C1 measured by ISTRa were compared. In the preliminary tests the displacement of C1 under maximal loading was approximately $22.5 \pm 1.5 \%$ less than that of the compressive element. In the series, where the steel plate was put on the sacral base, the displacement of C1 was $7.6 \pm 7.7 \%$ less than the displacement of the compressive element. This confirms the assumption that the plate enlarged the area of the application of the force, decreased the pressure in the contact area and reduced deformation of the surface of the model.

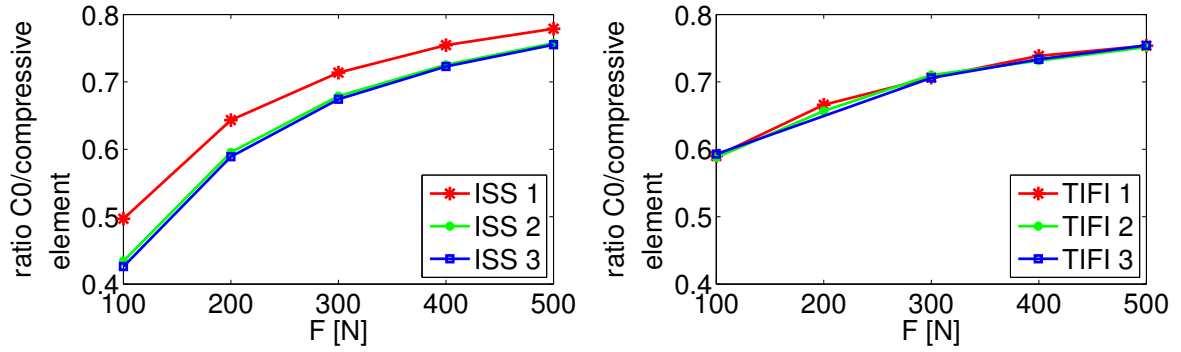


Fig. 4.5: Ratio of displacement of the compressive element and the point C1.

Tab. 4.3: Displacement of the compressive element (CE) and the point C1.

Meas.	Force [N]	Disp. of CE (DIC) [mm]	Disp. of CE (Ext.) [mm]	Disp. of C1 (DIC) [mm]	Ratio CE (DIC)/CE (Ext.)	Ratio C1 (DIC)/CE (Ext.)
ISS 1	100	0.41454	0.40837	0.2097	1.0151	0.5135
	300	1.0402	1.0166	0.75051	1.0232	0.7383
	500	1.6371	1.6016	1.2854	1.0222	0.8026
ISS 2	100	0.48207	0.47488	0.21435	1.0151	0.4514
	300	1.0753	1.0554	0.73791	1.0189	0.6992
	500	1.6457	1.6139	1.2562	1.0197	0.7784
ISS 3	100	0.49495	0.4878	0.21785	1.0147	0.4466
	300	1.0842	1.0661	0.74013	1.017	0.6942
	500	1.6498	1.6201	1.2559	1.0183	0.7752
TIFI 1	100	0.8749	0.85237	0.52229	1.0264	0.6128
	300	1.6602	1.6269	1.1781	1.0204	0.7241
	500	2.3721	2.3282	1.7915	1.0188	0.7695
TIFI 2	100	0.94317	0.94004	0.5622	1.0033	0.5981
	300	1.6973	1.6891	1.2142	1.0049	0.7188
	500	2.3815	2.3652	1.7961	1.0069	0.7594
TIFI 3	100	0.96783	0.94723	0.58205	1.0218	0.6145
	300	1.7232	1.6913	1.2238	1.0189	0.7236
	500	2.3964	2.3641	1.8139	1.0137	0.7673

According to the data in tab. 4.3, the difference between results obtained from the DIC software and the extensometer during these preliminary measurements was $1.66 \pm 0.63\%$. The decrease of the accuracy when compared to the above mentioned measurements was caused by different resolution of the compressive element in the images. Its width in pixels in these measurements was approximately 2.5 times smaller than in the first serie where the compressive element covered the whole field of view.

Even though two fixation techniques were used in these tests, the results have only informative character and they are not included in the comparative study. The main task of these experiments was to test the experimental setup, not to compare the fixators and so only a single pelvic model was used for all these tests.

4.2.3 Coordinate System in the DIC software

Coordinate system in the utilised DIC software was created during the calibration of cameras. Its origin and orientation of the axes were set based on the position of the calibration target at the moment when the first image used for the calibration was acquired. As the calibration was done manually, the coordinate system was unique for each serie of measurements because the cameras were calibrated before each serie.

In the preliminary tests the compressive element was a part of the acquired images. As the compressive element was set to move vertically, it was possible to set a vertical axis and to compute vertical displacements of selected points. Tab 4.4 shows total and vertical displacement of points C0 and C1 (point locations are shown in fig. 4.4). The vector of displacement and its vertical component is computed for both points. The angle between displacement vector of the point C0 and displacement vector of the compressive element differs from the angle between displacement vector of the point C0 and displacement vector of the compressive element. This indicates a complex spatial motion of the model.

4.3 Analysis of Selected Fixators

For the comparative study focused on four pelvic fixators, a serie of measurements was performed on the models. In order to obtain as comparable results as possible, each model was put through the same set of experiments. They were realized under the same conditions, using the same work flow.

4.3.1 Performed Measurements

Each measurement was recorded by two systems - the DIC software and the testing machine. Both of them produced a set of data that were further analysed.

When the testing machine was activated, the compressive element was located about a millimeter above the model. There was a 40 s pause before the measurement started. In this pause, several pre-images capturing the state of the model before loading were recorded by the DIC software. After 40 s the compressive element started to move. In the moment when it touched the model, the loading speed was regulated so as to keep the prescribed rate 150 N/min. When the force increased to the prescribed maximum, decreasing started with the same speed. In the end of the measurement the compressive element returned to its initial position so as not to touch the model.

The measurement was repeated ten times with a five minutes interval between the tests. Images were acquired by the DIC software with the frame rate 0.1 Hz, which corresponded to the increase/decrease of the force by 25 N.

Intact models

Before the fracture was created, the intact models were loaded so as to reveal eventual defects or differences between the models which could influence the measurements of

Tab. 4.4: Total displacements of points C0 and C1 and their displacement in vertical direction at applied load 500 N. Table contains data recorded by extensometer (Ext.) and results from DIC analysis (DIC).

Meas.	Force [N]	C0 total [mm]	C0 vertical [mm]	C0 Angle [deg]	C1 total [mm]	C1 vertical [mm]	C1 Angle [deg]
ISS 1	500	1.2854	1.2752	7.2092	1.2888	1.2609	11.9447
ISS 2	500	1.2562	1.2468	6.9836	1.2646	1.2416	10.93
ISS 3	500	1.2559	1.2459	7.2316	1.264	1.2417	10.7814
TIFI 1	500	1.7915	1.7877	3.72	1.7721	1.7429	10.4148
TIFI 2	500	1.7961	1.79	4.7322	1.7691	1.7442	9.641
TIFI 3	500	1.8139	1.8074	4.8477	1.7932	1.7662	9.9549

fractured models. During each measurement, load force up to 300 N was applied to the model. According to the previous measurements it was found that the model was not macroscopically damaged for applied loads up to 600 N. To minimise the risk of the eventual microscopic damage that could influence the tests of fixations, the maximal applied load in the intact state was set to 300 N only.

Fractured models

The behaviour of the fractured model was examined during a serie of measurements similar to the serie performed on the intact model, but the fractured models were loaded up to 500 N. As the pelvis in human body is loaded by about 60 % of its weight, 500 N corresponds approximately to pelvic loading in 80 kg body.

Under the real-life conditions (e.g. during walking), the sacrum is subjected to dynamic loads. However, loading in these measurements was quasi-static (as outlined above).

4.4 Data Processing and Evaluation

4.4.1 Data from the DIC Software

According to the data obtained from the DIC software, numerical values of displacements of several points on the sacral surface were evaluated and compared (Fig. 4.4). When the intact models were examined, just point C1 situated on the upper part of the median sacral crest was analysed.

The pairs of L and R points along the fracture, located under and over the sacral foramina, were analysed so as to know how the fracture responded to the applied load. The point C1 was used as an indicator of displacement allowed by a given fixator.

An output data file from the DIC software contains information about displacements u_i and coordinates of selected points in every acquired image and relative time t_i of acquisition of the images (Fig. 4.6 - upper part), where $i = 1, 2, \dots, n$ refers to the number of the image.

4.4.2 Data from Testing Machine

Voltage

Voltage was recorded by testing machine so as to synchronise the testing machine and the DIC software. There appeared a peak in voltage at the instant when the third image was acquired by the DIC software (Fig. 4.6). Time of the signal T_s measured by the testing machine corresponded to time t_3 measured by the DIC software. This allowed to assign synchronised time t_{sync_i} measured by testing machine to each image. It was set that the time of acquisition of the third image

$$t_{sync_3} = T_s,$$

which implies

$$t_{sync_i} = T_s - t_3 + t_i.$$

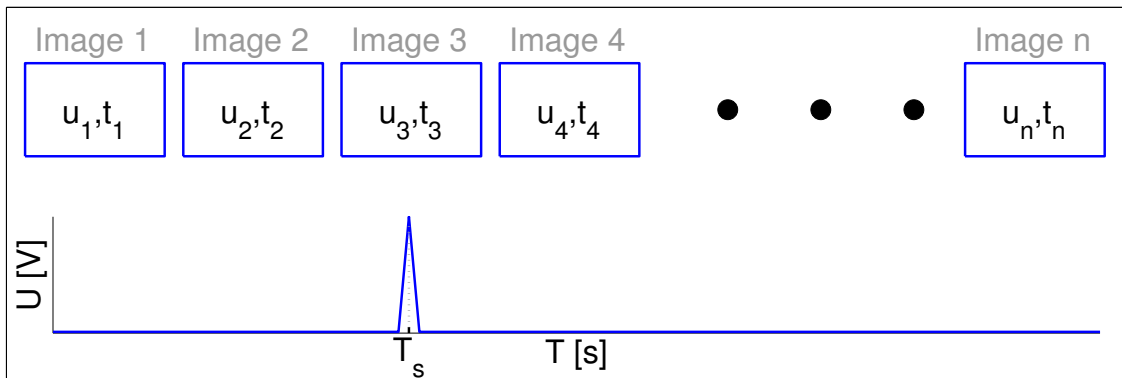


Fig. 4.6: Data processing procedure - time synchronisation

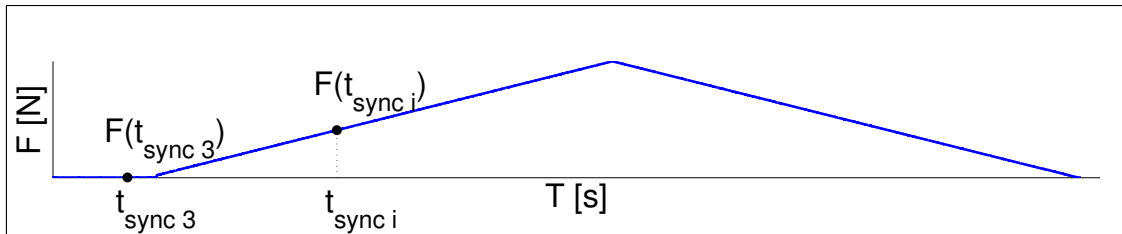


Fig. 4.7: Data processing procedure - applied load

Force

When all the images have assigned a time t_{Sync_i} , the magnitude of load applied at the instant of the DIC image acquisition can be obtained as

$$F_i = F(t_{Sync_i}), \quad (4.1)$$

where F is a magnitude of applied load recorded by testing machine (for more detail see Fig. 4.7).

Displacement

The displacement of the compressive element at the moment when the DIC images were acquired was detected in similar way as the applied load. As the compressive element was not touching the surface of the model in the beginning of the experiment, there was some movement before the compressive element touched the model and the loading started (Fig. 4.8a, point no. 2). Therefore, data from extensometer were recomputed so that the displacement in the moment of the contact was set to zero.

Data progress in time

When the evolution of force in time is displayed, there can be detected three specific points in the image in the most of the measurements

Point no. 1: **Beginning of the measurement.** The compressive element starts moving.

Point no. 2: **Contact.** The compressive element touches the model and the loading starts.

Point no. 3: **Stabilisation.** The testing machine has prescribed load which influences the speed of movement of the compressive element. As there is no force before the first and the second above mentioned point, the machine sets higher speed of movement of the compressive element. When it touches the model, it needs some time to adjust and stabilise its speed.

Ordinary evolution of displacement and force is shown in fig. 4.8a. It does not bring any complication in the detection of those three points.

In some of the measurements there appeared an acute increase of the displacement between the second and the third point (Fig. 4.8b). This might have been caused by a

slight change of position of the steel plate, however the exact cause of this effect was not studied.

In some other measurements there can be seen a noise that appears in the second point (Fig. 4.8c). It is a temporary effect that might have been caused by quivering of the steel plate before its stable position was found. However, in all the above mentioned cases all the three points can be identified.

Problem comes when there appears a noise in the first point, i.e. when the compressive element started moving (Fig 4.8d). This event occurred in approximately 12 % of the measurements. The assumed reason of this noise is that at the beginning of the movement the part of the testing machine that held the compressive element quivered, which influenced both the measured displacement and force.

In these cases the second point that is necessary for assignment of the displacement of the compressive element at the instant when it touched the model was not detectable. These measurements were excluded from analysis performed in section 4.2.2. However, they were not excluded from the comparative analysis of fixation techniques, because the other data (voltage, applied force) were not influenced by this noise.

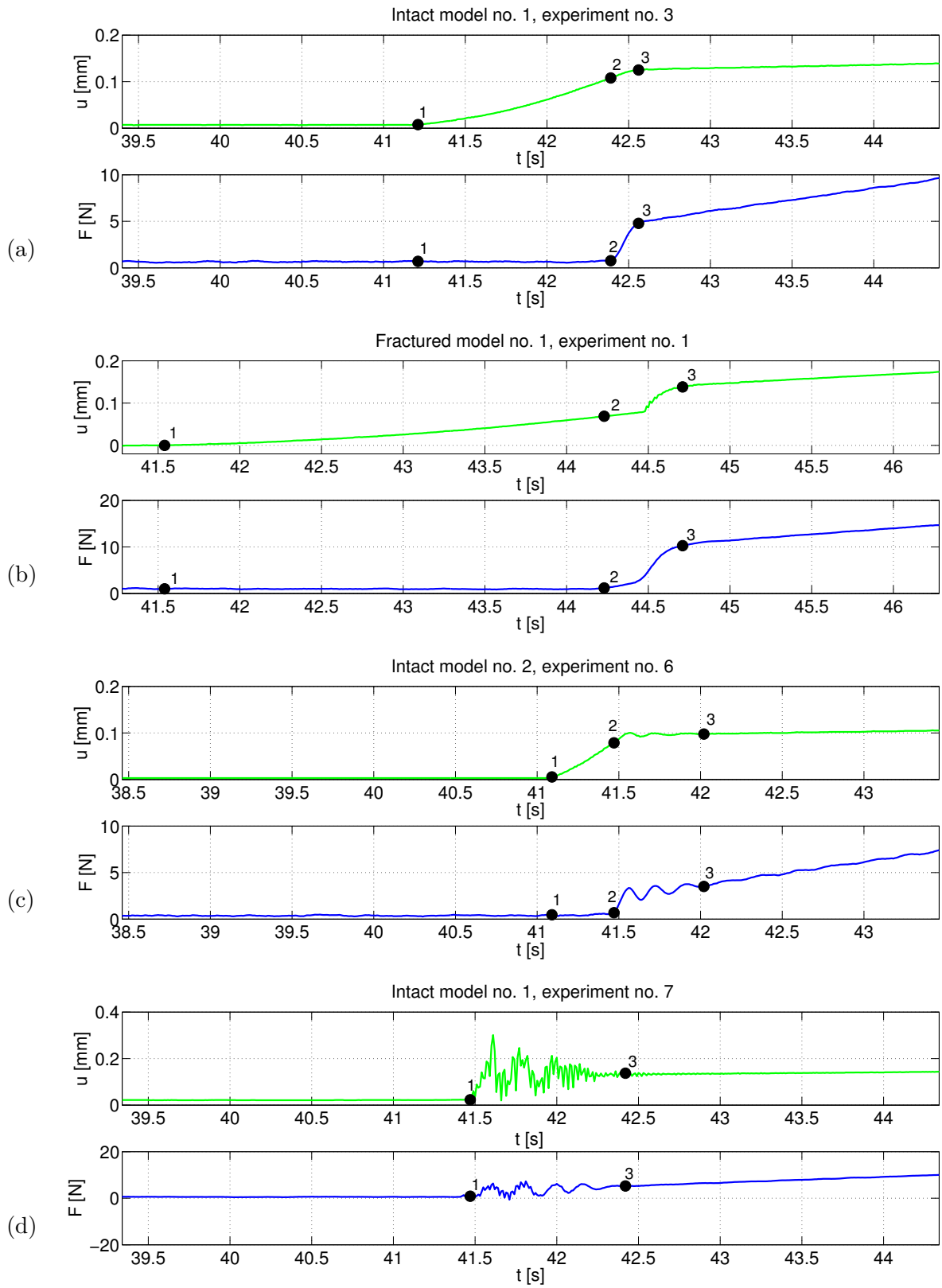


Fig. 4.8: Different progress of data obtained from extensometer. (a) No noise, (b) Creeping, (c) Insignificant noise, (d) Significant noise.

RESULTS OF COMPARATIVE STUDY

5

This chapter brings results of the comparative study that dealt with for sacral fracture fixation techniques. Their stability was evaluated based on the stiffness of the models.

5.1 Intact Models

Data from all the measurements were evaluated, except for the fourth measurement of the fourth model (prepared for application of SB) which did not bring usable results.

In fig. 5.1 are shown the force-displacement curves of the point C1. Data from the second measurement of each serie are displayed. It is obvious that in the intact state the force-displacement curve of all models is approximately linear.

The stiffness of the model was analysed using data corresponding to the applied load 150-300 N. The data in given interval were approximated by a straight line using the least squares method. The stiffness of the model was computed as the slope of this line.

The results are given in tab. 5.1. The data show that there were significant differences among the models.

The difference in stiffness may be caused by the structural differences of the utilised models and by different mounting to the stand leading to various levels of prestress. Therefore, the behaviour of the intact model must be taken into account when the data of fractured model are evaluated.

5.2 Fractured Models

As in the intact models analysis, a linear part of the force-displacement relationship could be identified for higher loads and a stiffness of the treated fractured models was computed. Based on fig. 5.2, linear part of the data was identified and approximated by a straight line. Data from the second measurement of each serie are displayed in the image.

The force-displacement curve of models treated with ISS and SB is approximately linear. At the model treated with TIFI there is notable nonlinear shape of the curve at the beginning of the measurement. However, for higher applied force the curve become linear. The model treated with TP has nonlinear time-displacement curve in the area of maximal applied load in the most of the measurements (see fig. 5.3c, the reason is discussed below). The interval of applied load where the curve is linear for all the measurements of all models was set as 250 - 450 N. Computed stiffness is given in tab. 5.1.

When the data of intact models and fractured models treated with given fixators are compared, it is obvious that the largest decrease of stiffness (35.4 %), which means the largest decrease of stability of pelvic girdle, is tolerated by ISS. Better stability is provided by TP (23.1 % decrease), and TIFI (21.8 %). By far the best stability is provided by SB (2.6 % decrease).

In fig. 5.3 there is shown the force-displacement curve of each model in the intact state and its force-displacement curve after stabilisation of created fracture. The slope of the curve of the fourth model did not change significantly after the stabilisation by SB. In the most of the measurements of the model treated with TP there is visible an unexpected movement of the model in the area of maximal loading. This effect was observed also at all the L points and it is likely related to the topology of the fracture of this particular model.

Another important aspect for evaluation of stability provided by the fixators is the behaviour of the fracture when the pelvis is loaded. Relative displacements between pairs of L and R points (Fig. 4.4) were computed. The values for each pair are shown in fig. 5.4. When compared TIFI, ISS and TP, the width of the gap between both sides of the fracture varied from 0.697 mm to 0.733 mm in the upper part (points L1-R1), and it varied from 1.413 mm to 1.52 mm in the lower part (points L6-R6). The gap at model stabilised by SB was significantly narrower, 0.051 mm in the upper part and 0.521 mm in the lower part.

The above mentioned characteristics of fractures are depicted in fig. 5.5. The contours of the fracture are highlighted there in the state with no loading, state with maximal loading in the first measurement and state with maximal loading in the last measurement. It is obvious that for the model treated with ISS the gap between both sides of the fracture is wider than in case of any other fixator.

According to the results from all analysed comparative aspects it is obvious that SB stabilised the fractured sacrum significantly better than the other fixators which behaved similarly. This was mostly caused by extremely tight fixation, which induced a significant compression in the region of the fracture. Such a compression is not suitable in real patients, however it was hard to control the level of compression during application of SB in the treated model.

Tab. 5.1: Stiffness of the models in intact state and at fractured models treated with given fixator.

Model	Intact model $\left[\frac{\text{N}}{\text{mm}}\right]$	Fixator	Fractured model with fixator $\left[\frac{\text{N}}{\text{mm}}\right]$	Ratio Fractured/Intact
1	626.70 ± 7.50	TIFI	489.93 ± 24.23	0.782
2	687.39 ± 7.47	ISS	444.37 ± 3.01	0.646
3	523.93 ± 7.47	TP	403.03 ± 8.59	0.769
4	520.77 ± 10.91	SB	507.15 ± 6.07	0.974

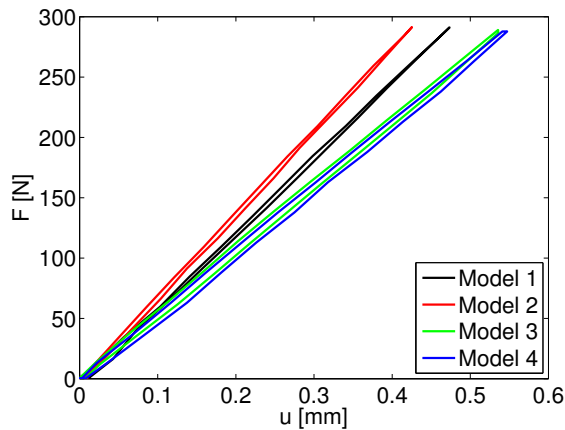


Fig. 5.1: Force-displacement curve of the models in the intact state.

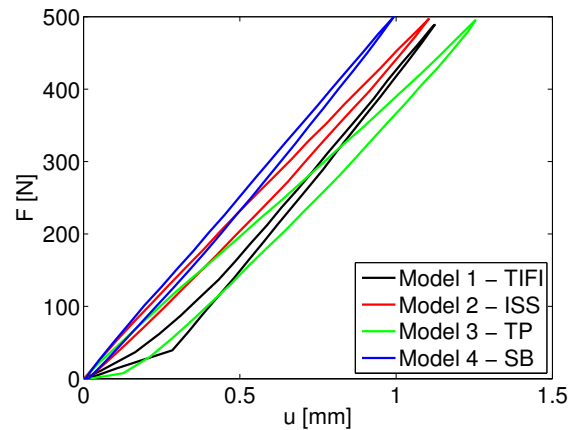


Fig. 5.2: Force-displacement curve of the fractured models treated with given fixator.

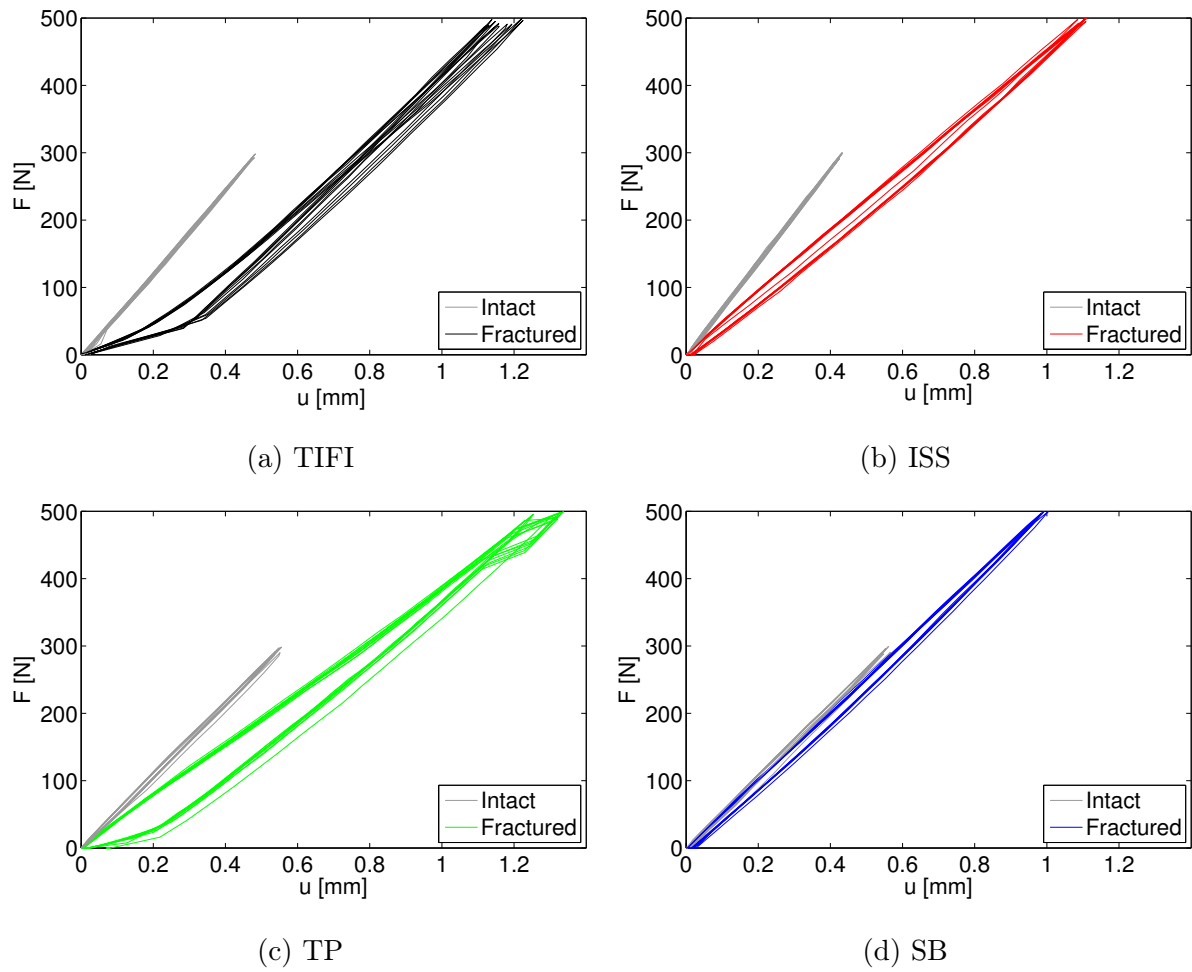


Fig. 5.3: Stiffness of the models in the intact state and of fractured models treated with given fixator.

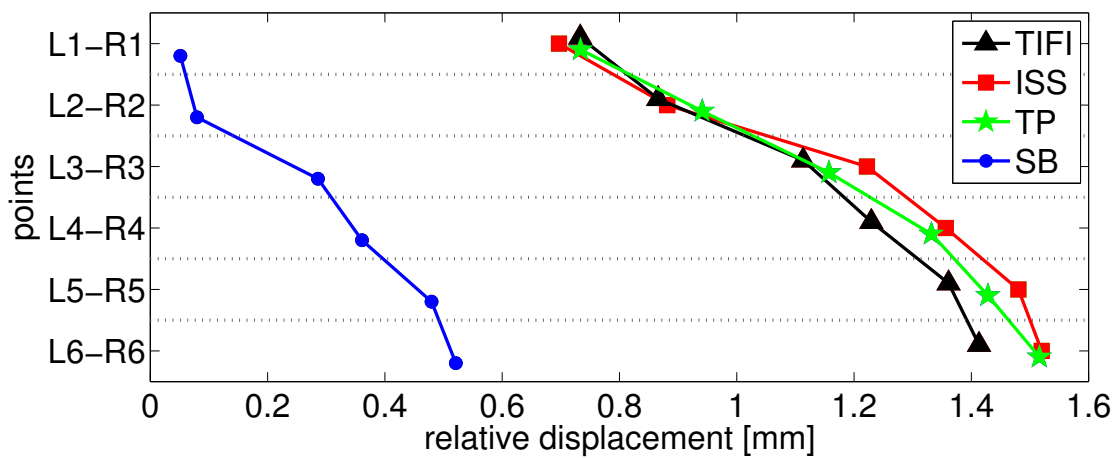
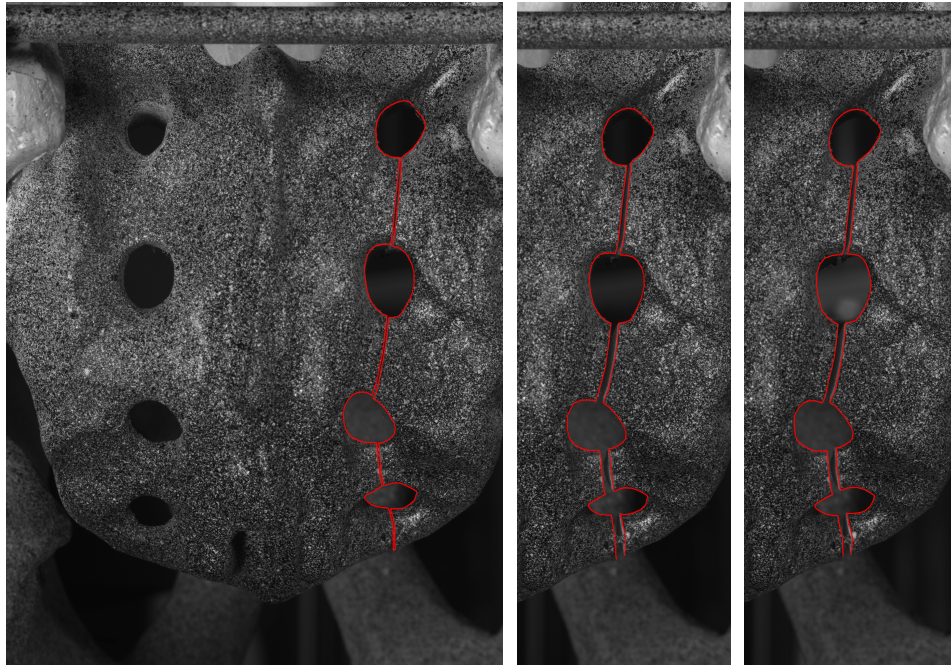


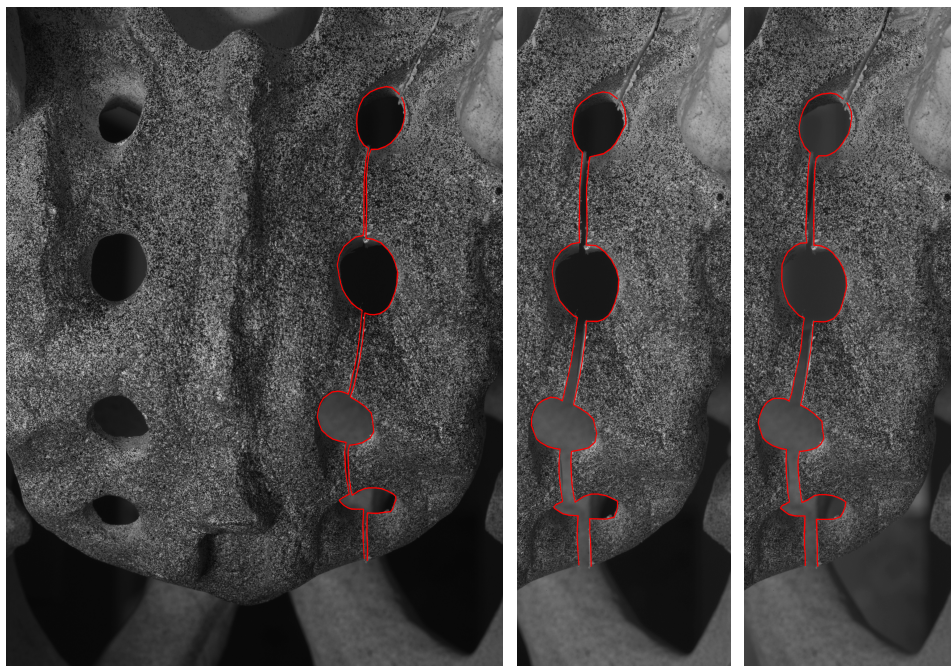
Fig. 5.4: Relative displacement of both sides of the fracture

Distinctions of particular measurements that influenced the accuracy of results were identified. The first variation was caused by unequal models. Experiments performed on intact models revealed that the pelvic models differed in their material response. Another possible source of inaccuracy arose during mounting of the pelvic models into the steel stand. Slight difference in positioning of the steel artificial femoral heads which supported the model led to different prestress in the models. The last source of variations in results was the contour of the surgically created fracture which differed among the models and could have influence the resulting relative displacement of the both parts of the fractured bone.

Results for ISS and SB in this study are in agreement with the study performed by Gorczyca et al. [26] where SB was proven to provide higher strength than ISS. When TIFI and ISS are compared, better stability is obtained by using TIFI which confirms results of study performed by Dienstknecht et al. [23]. Both Chen et al. [25] and Kobbe et al. [20] came to conclusion that TP has similar functional outcome as ISS. In this study TP stabilised the fracture better than ISS. However, Kobbe et al. used different comparative criterion as they retrospectively evaluated healing process at patients with treated fractures and their results are based on Pelvic Outcome Score of patients [20].

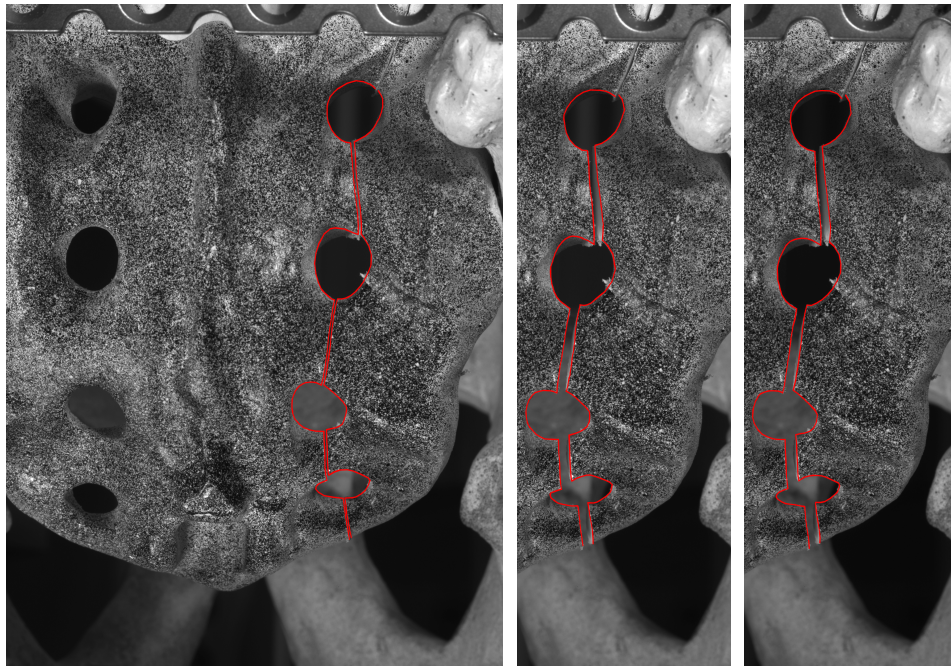


(a) TIFI

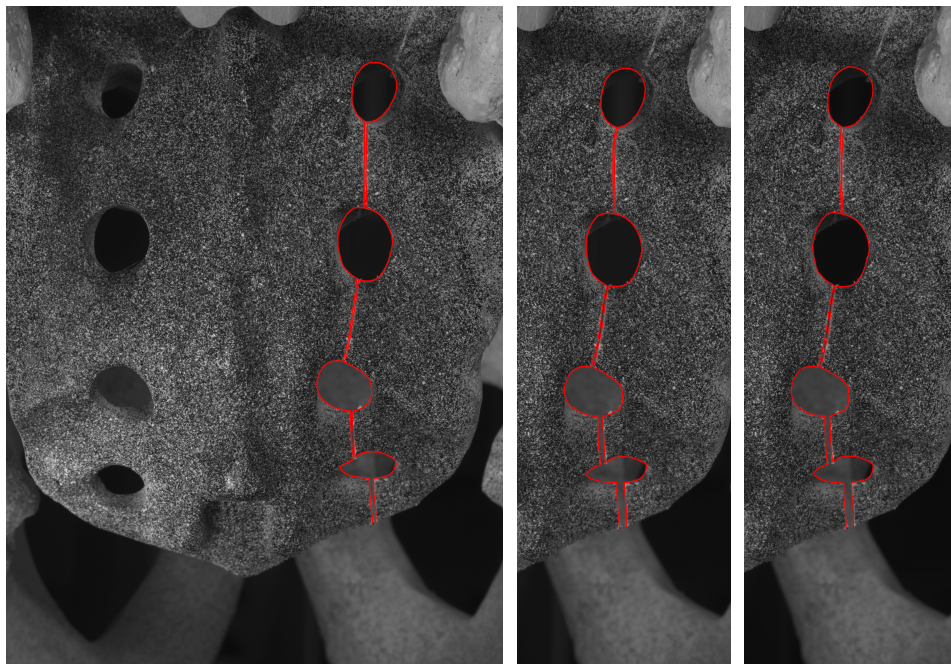


(b) ISS

Fig. 5.5: Highlighted contours of fracture and sacral foramina. Unloaded state in the first cycle (left), maximal loading in the first cycle (middle), maximal loading in the last cycle (right).



(c) TP



(d) SB

Fig. 5.5: Highlighted contours of fracture and sacral foramina. (Continued)

6

CONCLUSION

In the first part of this study, experimental procedure and methodology for pelvic models testing was devised and its suitability for the measurements was tested and verified. The photogrammetric software utilised for experimental data processing was examined in detail. Its functionality was tested in a series of measurements and the detected accuracy was discussed.

The second part of the study experimentally investigated mechanical behaviour of four fixators used for treatment of unstable vertical sacral fractures (Denis type II fractures [7]).

The results of this study suggest that the lowest stability was provided by two iliosacral screws where the fractured and treated model showed 35.4 % decrease of model stiffness. The transiliac plate caused decrease by 23.1 % and the transiliac internal fixator by 21.8 %. The decrease of stiffness by 2.6 % was encountered for two sacral bars . However, results of measurements of models treated with sacral bars were highly influenced by excessive compression of the fracture. The serie of measurements of fractured model stabilised by sacral bars will be repeated so as to have data of sacral bars comparable with those of the other fixators.

The results are in agreement with results of other comparative studies, for example with Dienstknecht et al. who compared transiliac internal fixator to iliosacral screws [23], Kobbe et al. and Chen et al. who compared transiliac plate to iliosacral screws [20, 25] and Gorczyca et al. who compared sacral bars to iliosacral screws [26]. The added value of this study is that it brings direct comparison of all four fixators.

In addition, results obtained from this study could be used for validation of numerical models of sacral fixation techniques that are being developed at the University of West Bohemia.

A.1 Calibration Target Analysis

The software was designed in Matlab [38] for analysis of chessboard calibration target. It detects corners of the squares based on colour contrast between adjacent squares. When the corners are identified, the images are correlated.

The user specifies the size of the grid (number of corners) to be exported and marks

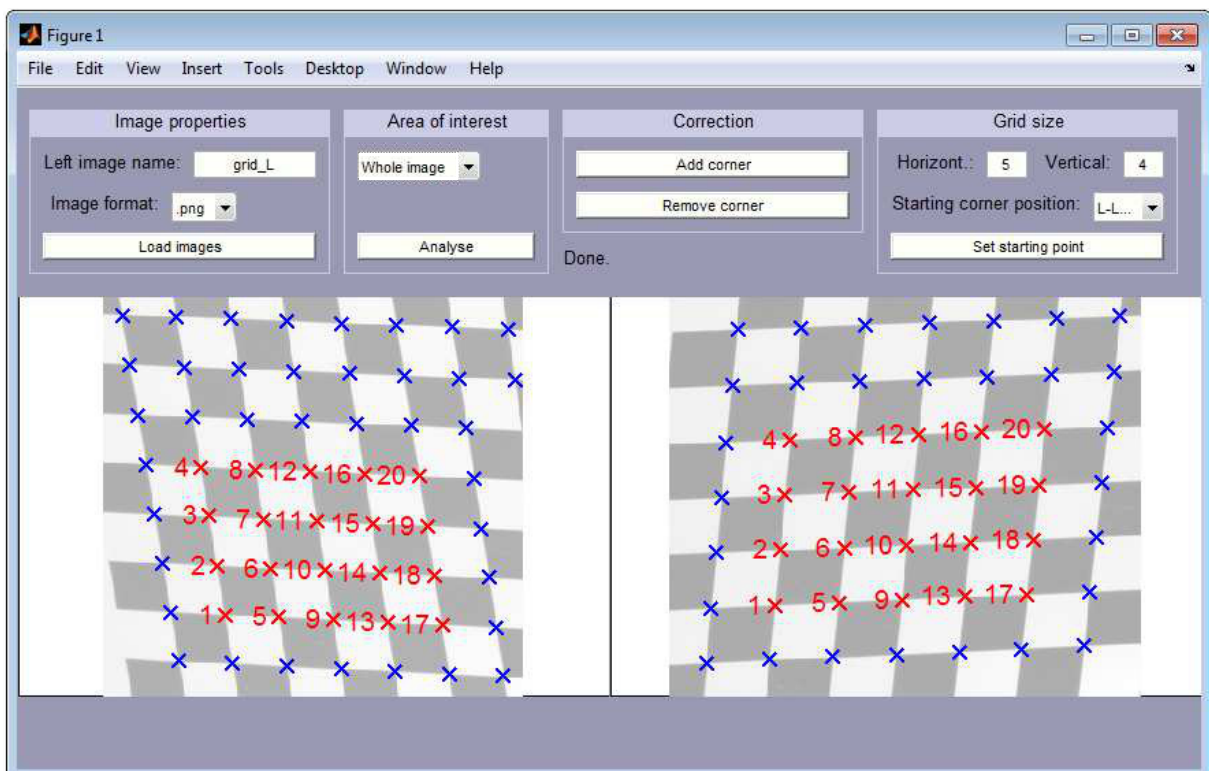


Fig. A.1: Chessboard - GUI

the position of the starting corner. In case of incorrect analysis, the user is allowed to remove or add corners manually.

A.2 Centre of Gravity Detection

This semi-automatic software was created in Matlab [38] for computation of centre of gravity of given object. It was designed for the analysis of measurements where two cameras were used for image acquisition. The output of this software is a data matrix for each image containing coordinates of centre of gravity of all objects.

The user marks the approximate position of objects in both images (for example dark spots on the surface of the model in analysis displayed in fig. A.2). The software then detects each object and computes its centre of gravity.

When the object cannot be detected because of poor image quality or some local complications, such as low contrast, shadows or noise in the area of interest, the centre of



Fig. A.2: Centre of gravity - GUI

gravity can be set manually.

The software offers the possibility of analysis of a serie of images capturing the progress of a measurement. Small displacements are assumed between each two following steps.

Modified version of this software is suitable for fully automatic analysis of images where only the area of interest is captured. It detects all objects in the image and computes their centre of gravity.

REFERENCES

- [1] <http://orthoinfo.aaos.org/topic.cfm?topic=a00223>
- [2] Pohlemann, T. (2000). Pelvic ring injuries: assessment and concepts of surgical management. In T. P. Rüedi, W. M. Murphy (Eds.), *AO Principles of Fracture Management* (395-418). Davos: AO Publishing.
- [3] Gray, H. (1913). *Anatomy, Descriptive and Applied*. Philadelphia: Lea & Febiger.
- [4] <http://www.innerbody.com/anatomy/skeletal/lower-torso/pelvis>
- [5] <http://www.methodistorthopedics.com/sacral-insufficiency-fractures>
- [6] Van de Graaff, K. M. (2002). *Human Anatomy, Sixth Edition*. Boston: McGraw-Hill.
- [7] Fakler, J. K. M., Stahel, P. F., Lundy, D. W. (2007). Classification of Pelvic Ring Injuries. In W. R. Smith, B. H. Ziran, S. J. Morgan (Eds.), *Fractures of the Pelvis and Acetabulum* (11-26). New York: Informa Healthcare.
- [8] Fakler, J. K. M., Pallister I., Stahel, P. F. (2007). Surgical Approaches for Pelvic Ring Injuries. In W. R. Smith, B. H. Ziran, S. J. Morgan (Eds.), *Fractures of the Pelvis and Acetabulum* (87-98). New York: Informa Healthcare.
- [9] <http://www.orthobullets.com/trauma/1030/pelvic-ring-fractures#4503>
- [10] Chong, K. H., DeCoster, T., Osler, T., Robinson, B., (1997). Pelvic Fractures and Mortality. *Iowa Orthop J.*, 17: 110–114.
- [11] Okpala, F. (2014). Measurement of Lumbosacral Angle in Normal Radiographs: A Retrospective Study in Southeast Nigeria. *Annals of Medical and Health Sciences Research*, 4(5): 757-762.
- [12] <http://www.sawbones.com/Catalog/Orthopaedic%20Models/Pelvis-Full/1301>

- [13] Kottner, R., Krystek, J. (2013). Vyšetření materiálových vlastností fyzického modelu pánve. Internal report, NTIS - New Technologies for the Information Society, University of West Bohemia.
- [14] An, Y. H., (2000). Mechanical Properties of Bone. In Y. H. An, R. A. Draughn (Eds.), *Mechanical Bone Testing of Bone and the Bone-Implant Interface* (41-64), Boca Raton: CRC Press.
- [15] Reilly, D. T., Burstein, A. H., Frankel, V. H. (1974). The elastic modulus for bone. *Journal of Biomechanics*, 7(3): 271-275.
- [16] Martens, M., Van Audekercke, R., Delport, P., De Meester, P., Mulier, J. C. (1983). The mechanical characteristics of cancellous bone at the upper femoral region. *Journal of Biomechanics*, 16(12): 971-983.
- [17] Marsh, J. L., Slongo, T. F., Agel, J., Broderick, J. S., Creevey, W., DeCoster, T. A., Prokuski, L., Sirkin, M. S., Ziran, B., Henley, B., Audigé, L. (2007). Fracture and dislocation classification compendium - 2007: Orthopaedic Trauma Association classification, database and outcomes committee. *J Orthop Trauma*, 21(10 Suppl): S1 133.
- [18] <http://ota.org/media/23066/97042.7Pelvis-S59-S67.pdf>
- [19] <http://www.dantecdynamics.com/istra-4d-shearography>
- [20] Kobbe, P., Hockertz, I., Sellei, R. M., Reilmann, H., Hockertz, T. (2012). Minimally invasive stabilisation of posterior pelvic-ring instabilities with a transiliac locked compression plate. *International Orthopaedics*, 36(1): 159-164.
- [21] Bodzay, T., Szita, J., Manó, S., Kiss, L., Jónás, Z., Frenyó, S., Csernátóny, Z. (2012). Biomechanical comparison of two stabilization techniques for unstable sacral fractures. *Journal of Orthopaedic Science*, 17(5): 574-579.
- [22] Dienstknecht, T., Berner, A., Lenich, A., Nerlich, M., Fuechtmeier, B. (2011). A Minimally Invasive Stabilizing System for Dorsal Pelvic Ring Injuries, *Clinical Orthopaedics and Related Research*, 469(11): 3209-3217.
- [23] Dienstknecht, T., Berner, A., Lenich, A., Zellner, J., Mueller, M., Nerlich, M., Fuechtmeier, B. (2011). Biomechanical analysis of a transiliac internal fixator. *International Orthopaedics*, 35(12): 1863-1868

- [24] Routt, M. L. C., Simonian, P. T., Inaba, J. (1997). Iliosacral screw complications. *Operative Techniques in Orthopaedics*, 7(3): 206-220
- [25] Chen, H., Liu, G., Fei, J., Yi, X., Pan, J., Ou, S., Zhou, J. (2012). Treatment of unstable posterior pelvic ring fracture with percutaneous reconstruction plate and percutaneous sacroiliac screws: A comparative study. *Journal of Orthopaedic Science*, 17(5), 580-587.
- [26] Gorczyca, J. T., Varga, E., Woodside, T., Hearn, T., Powell, J., Tile, M. (1996). The strength of iliosacral lag screws and transiliac bars in the fixation of vertically unstable pelvic injuries with sacral fractures. *Injury*, 27(8), 561-564.
- [27] Albert, M. J., Miller, M. E., MacNaughton, M., Hutton, W. C. (1993). Posterior pelvic fixation using a transiliac 4.5-mm reconstruction plate: a clinical and biomechanical study. *J Orthop Trauma*, 7(3), 226-232.
- [28] Hao, T., Changwei, Y., Qiulin, Z. (2009). Treatment of posterior pelvic ring injuries with minimally invasive percutaneous plate osteosynthesis. *International Orthopaedics* 33(5): 1435-1439.
- [29] Chen, B., Zhang, Y., Xiao, S., Gu, P., Lin, X. (2012). Personalized image based templates for iliosacral screw insertions: a pilot study. *The International Journal of Medical Robotics and Computer Assisted Surgery*, 8(4): 476-482.
- [30] Probe, R. A. (1999). Stabilization of posterior pelvic injury. *Operative Techniques in Orthopaedics*, 9(3): 161-176.
- [31] Salášek, M. (2014). Minimally invasive stabilization of posterior pelvic ring injuries with a transiliac internal fixator and two iliosacral screws: comparison of outcome and biomechanics.
- [32] McCormick, N., Lord, J. (2010). Digital Image Correlation. *Materials Today*, 13(12): 52-54.
- [33] McCurdy, P. G., Woodward, L. A., Davidson, J. L., Wilson, R. M., Ask, R. E. (1944). *Manual of Photogrammetry*. New York, Chicago: Pitman Pub. Corp.
- [34] <http://www.oxforddictionaries.com>
- [35] <http://www.collinsdictionary.com>

- [36] Sutton, M. A., Orteu, J., Schreier, H. (2009). Image Correlation for Shape, Motion and Deformation Measurements. New York: Springer.
- [37] Hartley, R., Zisserman, A. (2003). Multiple view geometry in computer vision. Cambridge: Cambridge University Press.
- [38] <http://www.mathworks.com/products/matlab>

LIST OF PUBLICATIONS

- [1] Salášek, M., Hartlová, J., Lobovský, L., Krystek, J., Pavelka, T., Křen, J., Ferda, J. (2015). Biomechanická studie transiliakálního vnitřního fixátoru, dvou iliosakrálních šroubů transiliakální dlahy a svorníků při stabilizaci transforaminálních sakrálních zlomenin. Národní kongres CSOT, Praha. (accepted for publication)
- [2] Lobovský, L., Salášek, M., Jansová, M., Hartlová, J., Krystek, J., Křen, J. (2015). Comparative study on various fixations of sacral bone injuries. 21st Congress of the European Society of Biomechanics, Praha. (accepted for publication)
- [3] Lobovský, L., Hartlová, J., Salášek, M., Krystek, J., Zemčík, R., Křen, J. (2014). Experimental investigation of deformations in human pelvis. In proc. Computational Mechanics 2014, Špicák. ISBN: 978-80-261-0429-2.
- [4] Hartlová, J., Lobovský, L. (2014). Experimental analysis of deformations in human pelvis. In proc. Studentská vědecká konference FAV 2014, University of West Bohemia, Plzeň. ISBN: 978-80-261-0364-6